Final Report: NSF-ATM-9896261

Sources and Sinks of Anthropogenic CO_2: Integrated Assessment Using Biogeochemical Modeling and Inversion of Atmospheric Tracer Transport

Project Activities and Findings

In collaboration with Prof. Jorge Sarmiento at Princeton University, we have developed a new method for quantitative assessment of the CO_2 budget of the atmosphere using measurements and modeling of stable isotope ratios. This has been accomplished by using combined data on CO_2 and ?^{13}C of atmospheric CO_2 derived from the GLOBALVIEW database (NOAA/CMDL, 2001). Please see the final report from the Princeton group, which is attached for your convenience.

Completion of this project was delayed significantly by the Principal Investigator's move from the University of California at Santa Barbara to Colorado State University in 1998.

One of the outstanding problems in inverse modeling of sources and sinks of CO_2 is the inability of the current observing network to reliably distinguish between terrestrial and oceanic uptake that each occur in similar latitude zones upstream of the observing locations. Terrestrial photosynthesis discriminates strongly against the heavier carbon isotope ^{13}C , while uptake into surface ocean water discriminates only slightly, providing an opportunity for more robust separability of these two major flux components within latitude zones. The two major aspects of the work that have been accomplished with NSF support are (1) the development of process-based models of stable isotope biogeochemistry that control the spatial and temporal patterns of isotopic fluxes within "basis regions" for the inversion; and (2) the development of a new inversion formalism to take advantage of the additional constraint represented by the isotope data. The forward model development included both terrestrial and marine components.

The specific tasks identified in the original proposal were as follows:

1. The development of a next-generation model of terrestrial biogeochemistry to predict the isotopic composition of CO_2 fluxes, including fractionation during photosynthetic carbon assimilation, the isotopic composition of various carbon pools of varying ages at multiple depths in the soil, and the isotopic composition of water in the terrestrial hydrologic cycle. This model will be derived from the Simple Biosphere Model (SiB2) at UCSB.
2. Development of a model of global air-sea exchange of $^{13}CO_2$ and $CO^{18}O$ at seasonal as well as annual time scales. This will be done in the context of the Ocean Biogeochemistry Model at Princeton University, by combining remotely sensed

seasonal ocean color data with existing physical, chemical, and biological ocean models.

3. Coupling of the above-mentioned terrestrial and marine flux models to three atmospheric circulation and chemical tracer transport models, to investigate the influence of surface isotope exchanges on the spatial and temporal variability of atmospheric CO_2 and its isotopes.
4. Inverse calculation of sources and sinks of atmospheric CO_2 using the results of the three atmospheric models coupled to the terrestrial and marine isotope BGC models, as constrained by atmospheric observations. The results from these inversions will also be used to suggest improvements to the component models.

Task 1 was completed under NSF support by Scott Denning and Neil Suits. Results are described in the attached paper, which will be submitted to *Global Biogeochemical Cycles* as soon as we have incorporated the comments of our coauthors. Major findings include unexpectedly large spatial and temporal variability in the isotopic fractionation within C_3 vegetation and a significant degree of interannual variability in the global flux-weighted mean discrimination of terrestrial ecosystems associated with ENSO-related climate variations. These results will have significant bearing on future calculations of interannual variability in terrestrial and marine carbon fluxes by isotopic deconvolution analysis.

Task 2 was completed by our colleagues at Princeton University (see their final report to NSF).

Task 3 has been completed in collaboration with Princeton. Many of the results are summarized in the attached paper. In general, the atmospheric models successfully predict the concentration and $?^{13}C$ of atmospheric CO_2 at the NOAA flask stations, both in terms of seasonal cycles and spatial variations. In addition, the model is able to predict local-scale fluctuations at the land surface (Fig 1) that arise from diurnal variability of

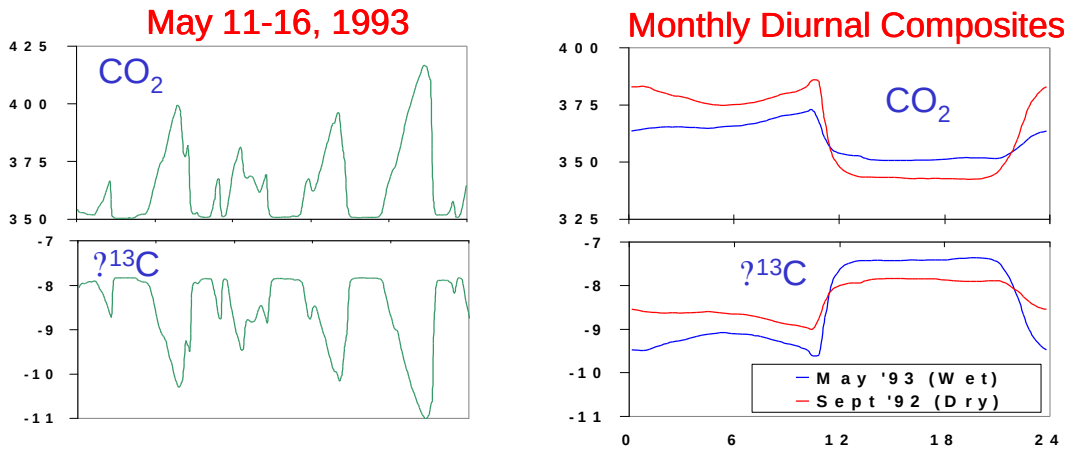

Fig. 1 - Simulated CO_2 and $?^{13}C$ in the canopy air space at a forest site in Brazil. This simulation used observed meteorology and assumes constant mixed layer conditions of 350 ppm and $?^{13}C$ + -7.8 ‰.

photosynthesis and respiration as well as changes in atmospheric stability and physiological stress. This allows the model result to be compared much more rigorously to data collected at field sites than any previous global model of isotope systematics.

Task 4 was completed primarily by our Princeton collaborators. Their results are summarized in detail in their final report to NSF. They have developed a new method to estimate fluxes and stable isotope ratios of the fluxes for continental and ocean-basin sized regions, and applied it to the carbon budget for 1993-1995. Their conclusion is that northern continents were absorbing about 2 x 10^{12} kg of carbon per year during this period while the tropical continents were emitting CO_2.

Training and Development

The support from NSF-MMIA has facilitated the training of a large number of people at Colorado State University. Two full-time graduate students (Theresa Krebs and Christopher Eller) were supported under the project, including both tuition and student stipends. In addition to classroom academic work, these students learned stable isotope biogeochemistry and participated in a major research effort. Chris Eller made major contributions to the global inverse modeling development, but left academia in 2001 to pursue a career in the information technology industry. Theresa Krebs is continuing to make progress on the development of a new model of isotope recycling within plant canopies, but is no longer supported by NSF. She is expected to receive her M.S. degree in 2002. Kevin Gurney was also supported under the project. He is a PhD candidate in the Graduate Degree Program in Ecology here at CSU, but is paid as a full-time Research Associate. He has learned about inverse modeling of the global carbon cycle and is now working on a major international inversion intercomparison project, also supported by NSF (TransCom, see http://transcom.colostate.edu). Dr. Neil Suits received two years of postdoctoral research training under this project. He was already well-versed in isotope biogeochemistry, but has learned to apply these principles to global models and to work with very large data sets.

In addition to student training and support, the project provided training and professional development to Marek Uliasz, John Kleist, Payam Askam-Ebrahimi, Connie Uliasz, and Ian Baker.

Outreach Activities

We have provided service and leadership to the emerging Biosphere-Atmosphere Stable Isotope Network (BASIN), a special project of the International Geosphere-Biosphere Programme/ Global Change and Terrestrial Ecosystems Project Office (see http://gcte-focus1.org/basin.html). This outreach has taken the form of attending the organizational workshop for BASIN, providing stable isotope fractionation maps to the BASIN scientists, and organizing a special meeting in 2002 to promote the use of stable

isotope information in carbon cycle inversions. Scott Denning also serves on the Community Climate System Model Biogeoichemistry Working Group, where he has helped steer the implementation of stable isotope systematics into the NCAR CCSM.

Simulating Seasonal and Spatial Variations in Global Concentrations and Carbon Isotopic Ratios of CO_2

N. S. Suits, A.S. Denning, J.A. Berry, C. Still, J. Kaduk, J. Sarmiento, S-M. Fan, J.T. Randerson

We use an ecophysiological model of the terrestrial ecosystem (SiB2), driven by observed meteorology provided by the European Center for Medium-range Weather Forecasts (ECMWF), and coupled offline to an atmospheric tracer-transport model (TM2), to generate seasonally and spatially varying concentrations and carbon isotope ratios of atmospheric carbon dioxide. Terrestrial $^{12}CO_2$ and $^{13}CO_2$ fluxes from SiB2 are then combined with similar fluxes produced by 1) fossil fuel burning and 2) exchange with the ocean as calculated in an ocean biogeochemical model. These total fluxes are prescribed to TM2 in order to predict seasonal and spatial variations in carbon isotope ratios of atmospheric CO_2, which are then compared to measurements from the Global Flask network. Predicted seasonal cycles of concentrations and carbon isotope ratios of CO_2 compare well with observations, although there are slight discrepancies in both magnitude and phase of these two parameters. A comparison of results of Keeling plots from the simulation and from data collected at sites from the NOAA Global Flask Network show that the simulation systematically underestimates $\delta^{13}C$ values of CO_2 contributing to variations in p CO_2 and $\delta^{13}C$ at these sites. Results indicate that seasonality in $\delta^{13}C$ of atmospheric CO_2 tends to enrich carbon isotopic ratios of living plant carbon over large areas of western continental Eurasia, while depleting it in the southern United States and northern Africa. Results further indicate that recycling of respired CO_2 in the canopy depletes carbon isotope ratios of plant carbon by a few tenths of a per mil (‰).

Introduction

Atmospheric CO_2 concentrations have been increasing for the past 150 years due to the activities of humans, such as combustion of fossil fuels and manufacture of cement. While the anthropogenic flux of CO_2 in the 1980s was approximately 5.5 ±0.5 Gt-C/year [IPCC, 2000], atmospheric CO_2 only increased at a rate of 3.2 ±0.2 Gt-C/year. Consequently, during this period there was a natural sink for nearly half of the anthropogenically added CO_2. However, the nature of this sink (or sinks), as well as their spatial and temporal distribution, is still a matter of dispute.

In general, sinks are divided geographically, and into oceanic and terrestrial exchange processes. Seasonal and spatial variations in atmospheric CO_2 concentrations are interpreted using numerical transport models to deduce the position and magnitude of large-scale sources and sinks [Fan et al., 1998; Bousquet et al., 1999a, 1999b; Rayner, et al., 1999]. The stable isotopic composition of CO_2 also contributes information on sources and sinks [Ciais et al, 1995a, 1995b; Enting et al., 1995; Rayner, et al., 1999], and, in particular, can help to distinguish marine from terrestrial fluxes. This is because CO_2 exchange between the atmosphere and terrestrial ecosystems is accompanied by large isotopic fractionations (5 to 25‰) [Deines, 1980], whereas exchange between the atmosphere and ocean involves isotope effects that are an order of magnitude smaller (1 to 2‰) [Mook et al, 1974; Wanninkhof, 1985]. Furthermore, because of the large and variable isotope fractionations during exchange with the terrestrial biosphere, as well as the magnitude of terrestrial CO_2 fluxes, carbon isotopic ratios of atmospheric CO_2 are particularly sensitive to changes in terrestrial ecosystems. Consequently, any attempt to accurately simulate seasonal variations in $\delta^{13}C$ of atmospheric CO_2 depends on a reliable model of carbon isotope systematics of the terrestrial biosphere.

In terrestrial ecosystems, the magnitude and carbon isotopic ratio of CO_2 fluxes is determined by rates of respiration and photosynthesis, as well as carbon isotopic discrimination during photosynthesis. These all vary seasonally and diurnally in response to changes in physiological state [Farquhar et al., 1982, 1988; Berry, 1988]. Changes in state are produced by variations in plant and soil water balance and the surface energy budget, i.e., partition of net radiation between latent and sensible heat fluxes. Environmental fluctuations such as these also produce and interact with atmospheric transport and turbulent mixing between the canopy and

the overlying atmosphere. Consequently, interactions between the physical conditions within the canopy and the biota control seasonal and diurnal variations in the magnitude and isotopic signature of terrestrial biospheric CO_2 fluxes. And therefore, validity of model results relies upon an accurate representation of the linkages between terrestrial photosynthesis, respiration, carbon isotope discrimination factors, heat and water fluxes, as well as turbulent processes within the canopy and interactions between the canopy and large-scale transport in the atmospheric [Denning et al, 1995, 1999].

Previous investigations of the influence of the terrestrial biosphere on $\delta^{13}C$ of atmospheric CO_2 have generally simplified characterization of carbon isotope discrimination by assuming ether that it is globally constant or the product of a annual flux-weighted zonal mean [Ciais et al, 1995a, 1995b; Enting et al., 1995; Fung et al., 1997; Rayner, et al., 1999]. Others have used physiologically based models of plant discrimination using monthly assimilation-weighted discrimination factors. In this study, we introduce carbon isotope calculations to an ecophysiologically based model of the terrestrial biosphere (SiB2) in order to predict the magnitude and carbon isotopic signature of CO_2 exchange between the terrestrial biosphere and the atmosphere. Carbon isotopic ratios of fluxes to and from the terrestrial biosphere are calculated each ten-minute time step using a multi-step model of diffusion and photosynthetic assimilation of canopy CO_2. Spatial and temporal variations in distributions of C3 and C4 plants are taken into account, as are diurnal changes in $\delta^{13}C$ of canopy CO_2, the source of the assimilated carbon. We test the accuracy of our simulation by comparing predicted concentrations and $\delta^{13}C$ ratios of atmospheric CO_2 to observations from the Global Flask Network. We also investigate the influence of dynamic relationship between the atmosphere and the terrestrial biosphere in determining $\delta^{13}C$ of plant carbon, as well as interannual variations in the carbon isotopic ratio of terrestrial fluxes.

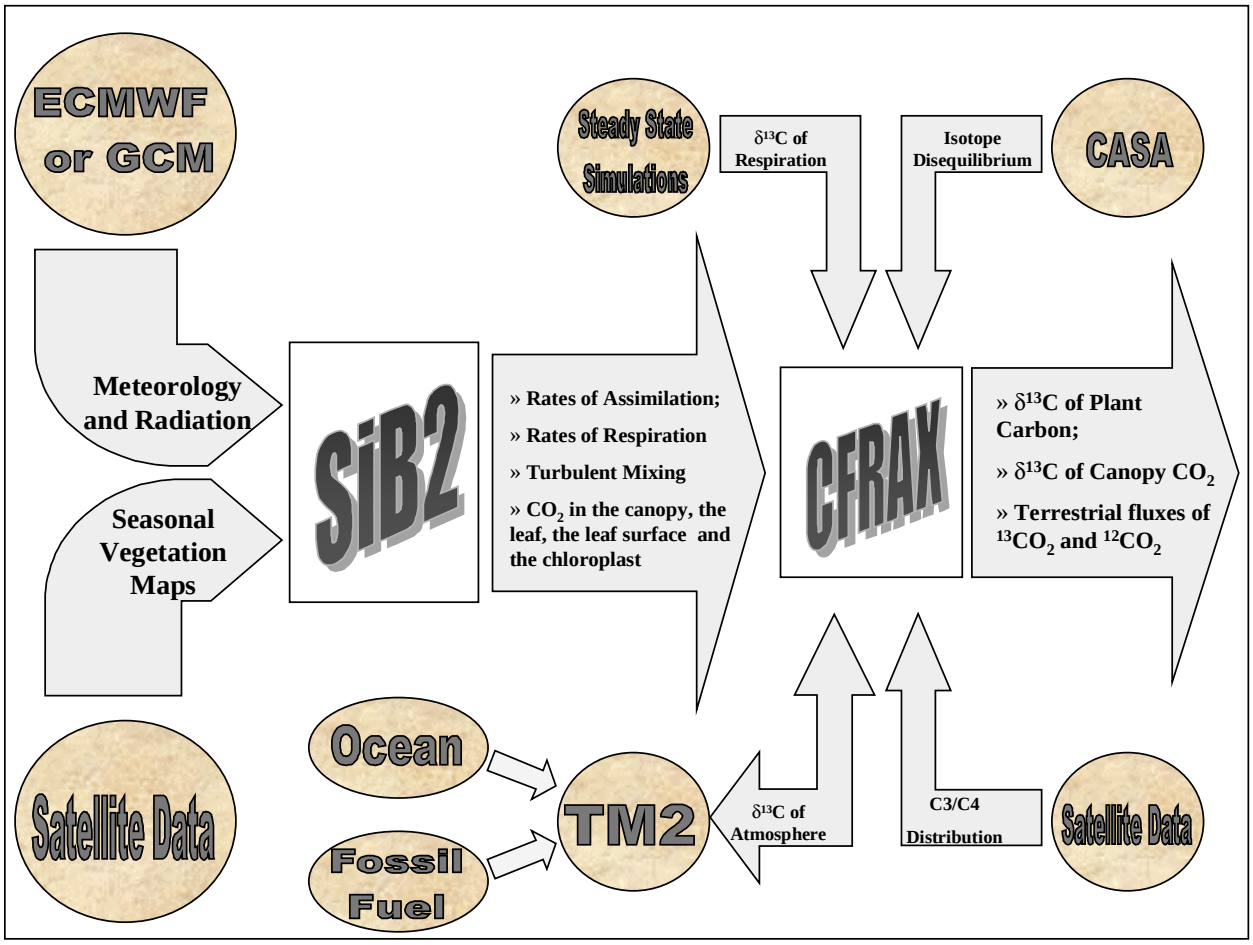

Figure 1. Structure of the present simulation. Arrows indicate the flow of information between components of the simulation. See text for details.

Method

Structure of the simulation

The present simulation is structured as follows (Fig. 1). SiB2 is driven by assimilated meteorology provided by the European Center for Medium-Range Weather Forecasting (ECMWF) with a 1° spatial resolution and a 6-hour time step. ECMWF provides 1) wind speed at 10 meters *height*, 2) temperature at 2 meters, 3) relative humidity at 10 meters, 4) total incident solar radiation, and 5) precipitation. Using this data, SiB2 calculates surface fluxes of sensible and latent heat, radiation, moisture, canopy aerodynamic properties and momentum for vegetated land points [Sellers et al., 1986, 1992a, b, 1996a; Randall et al., 1996]. Biome-specific

parameters are derived from processed satellite data and literature [Los et al., submitted]. These parameters include vegetation type, vegetation cover fraction and soil properties. Satellite data also specify time-varying phenological properties including leaf area index (LAI), the fraction of photosynthetically active radiation absorbed by the green canopy (FPAR), and canopy greenness fraction by processing the normalized difference vegetation index (NDVI) gathered from the Advanced Very High Resolution Radiometer red and near-infrared data. Seasonal variation in distribution of C4 plants is determined by monthly 1° X 1° maps (Fig 2) [Still et al., in preparation]. These maps were created by combining remote sensing products [Devries et al., 1999] with physiological modeling [Collatz et al., 1998], and modified using monthly maps of C3 and C4 agriculture. Carbon isotope discrimination by C3 plants is determined in a multistep process [Lloyd and Farquhar, 1994]. Concentrations and carbon isotopic ratios of CO_2 in the canopy, as well as CO_2 assimilated by plants, vary diurnally and seasonally as a result of changes in rates of photosynthesis and respiration, carbon isotopic ratios of those fluxes, as well as turbulent mixing between the canopy and the overlying atmosphere. Rates of photosynthesis and

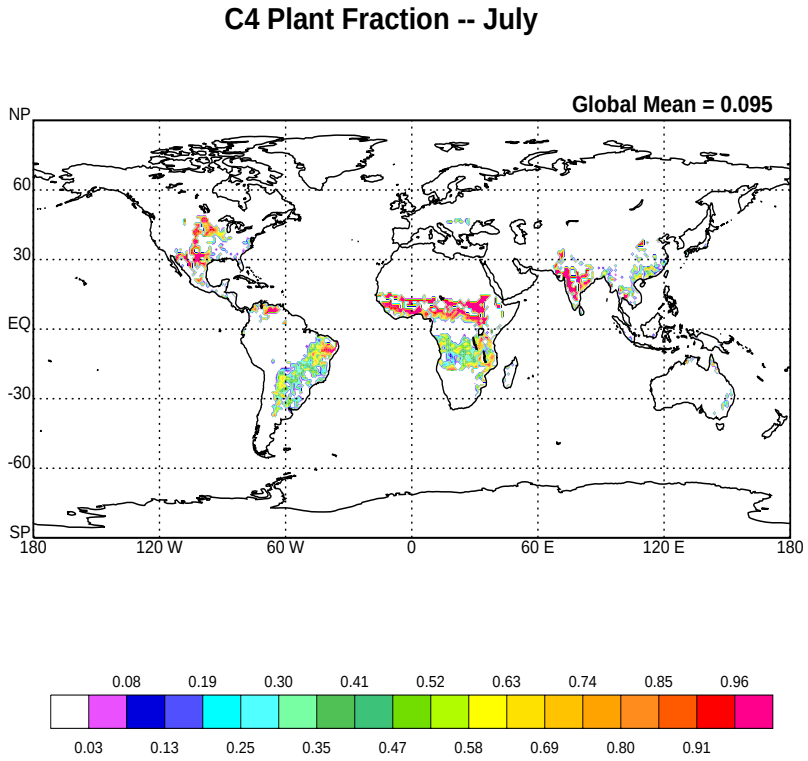

Figure 2. Global C4 plant fraction in July (Still et al., in prep.). Values range from 0 to 1 and represent the fraction of the vegetation that uses C4 photosynthesis for carbon assimilation.

respiration, carbon isotope discrimination and turbulent mixing are determined every 10 minutes. $\delta^{13}C$ of respired carbon is constant at the flux-weighted mean for each grid cell plus a biotic isotope disequilibrium offset due to the fact that soil organic matter is older than the above-ground biomass, and consequently was produced in an atmosphere enriched in ^{13}C relative to the present atmosphere. Spatial resolution in SiB2 is 1° X 1°.

A Simple Model of the Biosphere (SiB2)

Photosynthesis

The net rate of carbon assimilation due to photosynthesis (An) is a potential rate which is modulated by 1) enzyme kinetics (ω_c), 2) responses to varying light levels (ω_e), 3) the plant's ability to process the sugars and starches that are produced (ω_s), and 4) losses due to leaf respiration (R_1) [Farquhar, 1980; Collatz et al., 1991, 1992].

$$\mathbf{A_n = \min(\omega_c, \omega_e, \omega_s) - R_1}$$

(1)Stomatal conductance to water vapor (g_{lbl}), net carbon assimilation rate (A_n), and CO_2 concentration in the leaf boundary layer (C_{lbl}), i.e., at the leaf surface, are related by the equation

$$\mathbf{g_{lbl} = m\,(A_n\, h_{lbl})/C_{lbl} * p + b,} \qquad (2)$$

where h_{lbl} is the relative humidity at the leaf surface, p is atmospheric surface pressure, and m and b are empirically-derived parameters [Ball, 1988; Collatz et al. 1991, 1992]. Partial pressure of CO_2 in the canopy (C_a), at the leaf boundary layer (C_{lbl}) and in the stomatal cavity (C_{stoma}) are calculated according to the equation

$$\mathbf{A_n = (g_{stoma} / 1.6) * (C_{lbl} - C_{stoma})/ p = (g_{lbl} / 1.4) * (C_a - C_{lbl}) / p} \qquad (3)$$

g_{lbl} and g_{stoma} are coefficients of molecular diffusion of water vapor across the leaf boundary layer and through the stomata, respectively. And factors 1.4 and 1.6 relate diffusion coefficients of CO_2 to those of water vapor. Since ω_e and ω_c are functions of C_{stoma}, equations 1, 2 and 3 are

solved simultaneously for g_{lbl}, A_n, and C_{stoma} in an iterative scheme [Collatz et al., 1991]. Finally, CO_2 concentrations at the chloroplast (C_c) are then calculated as follows.

$$\mathbf{C_c = C_{stoma} - g_{mesophyll} * A_n}, \quad (4)$$

where $g_{mesophyll}$ is the coefficient of conductance for CO_2 between the stomatal cavity and the chloroplast, and is assumed to be linearly proportional to the Michaelis-Menten coefficient characterizing the enzymatically controlled maximum rate of photosynthesis.

Respiration

In SiB2, we assume that there are no changes in storage of soil carbon from year to year. Consequently, soil respiration is equal to canopy net assimilation, on an annual basis. Nonetheless, rates of ground respiration can vary widely from time step to time step, and are modeled as a function of soil moisture and temperature according to the method used by Raich et al. [1991]. The relative intensity of respiration (R^*) is defined as

$$\boldsymbol{R^* = 2.0^{\,Q_t} f(m)}, \quad (5)$$

where

$$\mathbf{Q_t = (T - 298)/10}, \quad (6)$$

$$\boldsymbol{f(m) = 0.2 + w_{sat}^{B}}, \quad (7)$$

$$\mathbf{B = [(w^{z_m} - w^{z_{opt}}) / (w^{z_{opt}} - 100)]^2}. \quad (8)$$

In the above equations, w is the fraction of soil space filled by water and T is the warmer of the surface soil temperature and the deep soil temperature. The variable w in (8) is the fraction of the pore space occupied by water in the root zone (middle layer) of the soil. w_{sat}, w_{opt}, and z_m are prescribed according to soil texture using values suggested by Raich *et al.* [1991]. Soil respiration rates are at a maximum for some optimum soil moisture (w_{opt}), and lower when conditions are either wetter or drier.

A dimensionless soil respiration rate, $r^*(t)$, is defined for each time step as

$$r^*(t) = R^*(t) / \sum_{1\,year} R^*(t)\Delta t \quad (9)$$

The CO_2 flux, R(t), from the soil due to respiration is computed from this dimensionless rate as

$$R(t) = r^*(t) \times \sum_{1\,year} An^*(t)\Delta t \quad (10)$$

Equation (10) represents the assumption of a local steady state for carbon storage in terrestrial ecosystems on an annual basis, so that the net annual flux of CO_2 is zero.

A Carbon Isotopic Model of the Canopy (CFRAX)

CFRAX uses output from SiB2 to calculate 1) kinetic isotope effects accompanying C3 and C4 photosynthesis, 2) carbon isotopic ratios of canopy CO_2 and assimilated plant biomass, and 3) the magnitude and carbon isotopic ratio of CO_2 fluxes between the canopy and overlying atmosphere (Fig. 3). The data required to make these calculations are 1) rates of respiration (Resp) and net photosynthesis (A_n), 2) concentrations of CO_2 in the canopy (C_a), at the leaf surface (C_s), within the stomatal cavity (C_i) and chloroplast (C_c), and 3) a coefficient of resistance to turbulent exchange between the canopy and the overlying atmosphere (r_a). The value of each variable is determined every ten minutes. The solution scheme is as follows. During each time step, CO_2 in the canopy is 1) removed by photosynthesis, 2) added to by respiration, and 3) exchanged with CO_2 in the overlying atmosphere as a result of turbulent mixing. The $\delta^{13}C$ value of assimilated carbon is determined by the $\delta^{13}C$ of canopy CO_2, plus an offset due kinetic isotope effects during photosynthesis (Δ_{PS}). $\delta^{13}C$ of respired CO_2 is the steady state $\delta^{13}C$ of plant carbon determined in the model, plus an offset due differences in $\delta^{13}C$ of living plant biomass and respired soil organic matter (SOM). Photosynthesis causes canopy CO_2 to become enriched in ^{13}C; respiration causes canopy CO_2 to become depleted in ^{13}C; and exchange between the canopy and overlying atmosphere tends to restore $\delta^{13}C$ of canopy CO_2 back to the background level of the atmosphere.

$$\frac{d}{dt}(C_{ca}\,\delta^{13}C_{ca}) = \frac{d}{dt}(Resp\;\;\delta^{13}C_{resp}) - \frac{d}{dt}(A_n\;\;\delta^{13}C_{PS}) + \frac{d}{dt}(1/r_a\;(C_m\,\delta^{13}C_m - C_{ca}\,\delta^{13}C_{ca})) \quad (11)$$

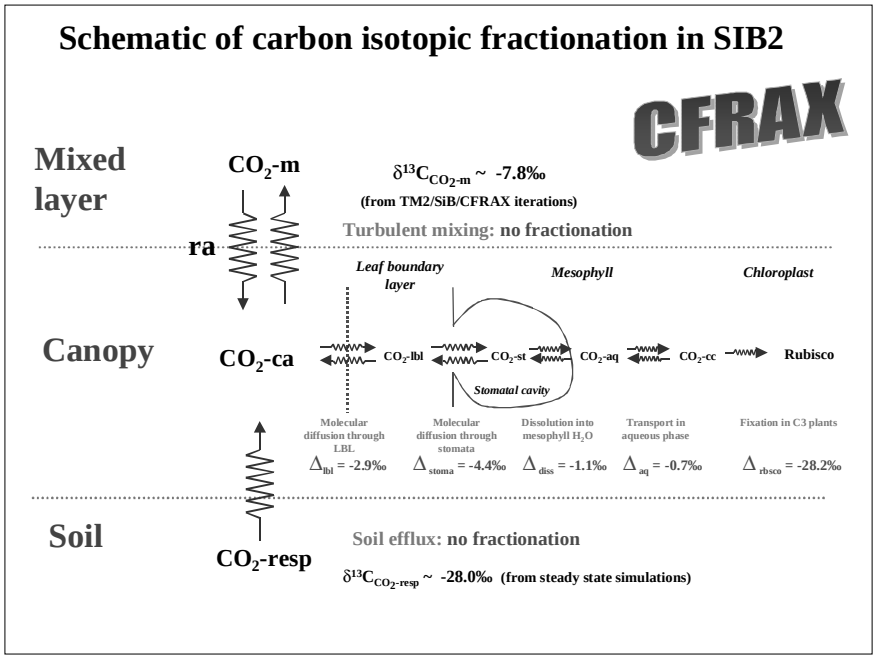

Figure 3. Structure of carbon isotopic calculations in SiB2. Arrows indicate carbon flow. Delta values express the kinetic isotope effects associated with each transfer [Craig, 1953; Mook et al., 1974; Farquhar, 1983; O'leary, 1984]. We assume that 5% of fixation by C3 plants occurs using PEPC, and consequently the net isotopic discrimination during C3 photosynthesis decreases by 2‰.

where $\delta^{13}C_{resp}$, $\delta^{13}C_{PS}$, $\delta^{13}C_{ca}$ and $\delta^{13}C_m$ are the carbon isotopic ratio of respiration, assimilation, the canopy and overlying atmosphere, respectively. C_{ca} and C_m are CO_2 concentrations in the canopy and overlying atmosphere. C_m and $\delta^{13}C_m$ can be calculated interactively in a GCM, kept constant at some mean value, or, as in this case, prescribed by a atmospheric transport model, which integrates the effects of net CO_2 fluxes between the atmosphere and 1) the ocean, 2) the terrestrial biosphere and 3) due to fossil fuel combustion.

Photosynthesis is associated with kinetic isotope effects that deplete the plant carbon in ^{13}C. Isotopic fractionation during photosynthesis is the sum of all isotopic effects during transport of CO_2 to the site of fixation, weighted by the concentration gradients associated with each step, plus the kinetic isotope effect accompanying enzymatic carbon fixation. We have adopted an approach similar to Lloyd and Farquhar [1994] in which transport in C3 plants is divided into 4 separate steps: (1) diffusion of canopy CO_2 across the laminar leaf boundary layer, (2) molecular diffusion through the stoma, (3) dissolution into mesophyll water, and finally (4) aqueous phase transport to the chloroplast.

$$\Delta_{C3} = \Delta_s \, C_{ca}/C_{ca} + (\Delta_i - \Delta_s) \, C_s/C_{ca} +$$

$$(\Delta_{diss} + \Delta_{aq} - \Delta_i) \, C_i/C_{ca} + (\Delta_{rbsco} - \Delta_{diss} - \Delta_{aq}) \, C_{cc}/C_{ca} \quad (12)$$

Δ_s, Δ_i, Δ_{diss}, Δ_{aq} and Δ_{rbsco} are kinetic isotope effects associated with transport through the leaf boundary layer, into the stomatal cavity, into solution, aqueous phase transport and fixation by rubisco, respectively. C_{ca}, C_s, C_i and C_{cc} are the corresponding CO_2 concentrations in the canopy, at the leaf surface, within the stomatal cavity and chloroplast.

C4 photosynthesis also discriminates against ^{13}C, but to a much lesser extent. In C4 plants, CO_2 is 'captured' in the stomatal cavity and transported to the site of enzymatic fixation with PEPC. Since nearly all of the CO_2 that reaches the site of fixation in C4 plants is assimilated, the only kinetic isotope effects that are expressed are those involved in transport. Consequently, in this model we assume that carbon isotopic discrimination in C4 plants is constant and equal to the isotope effect associated with diffusion through the stomatal pore, i.e.,

$\Delta_{C4} = -4.4‰$.

The resulting $\delta^{13}C$ values of carbon assimilated during each time step by C3 or C4 plants ($\delta^{13}C_{plant}$) is equal to the $\delta^{13}C$ of canopy CO_2, plus an offset due to isotopic discrimination during photosynthesis (Δ_{C3} for C3 plants, or Δ_{C4} for C4 plants). In ecosystems with a mixture of C3 and C4 plants, the photosynthetic discrimination is a C3/C4-weighted ratio of their respective isotopic discriminations (13).

$$\delta^{13}C_{plant} = \delta^{13}C_{canopy} + An_{C3} \, \Delta_{C3} + An_{C4} \, \Delta_{C4} \quad (13)$$

where An_{C3} and An_{C4} are the fraction of net assimilation accounted for by C3 and C4 plants, respectively.

Using δ-notation in mass-isotope balance calculations can lead to slight inaccuracies in the solutions because 1) δ values are not true ratios, and 2) transfer of mass from one reservoir with a specific δ value (δ_1) to another reservoir with a different δ value (δ_2) is not simply a matter of adding a certain amount of CO_2 with a carbon isotopic ratio of δ_1 to the second reservoir. Mass transfer is proportional to concentration gradients of the transferred species.

Differences in δ values between two reservoirs implies that the concentration gradients, and thus fluxes, of the two isotopically substituted species, e.g., $^{12}CO_2$ and $^{13}CO_2$, are also different. To avoid this imprecision we split CO_2 into the two separate reservoirs and fluxes by converting δ and Δ values into the concentrations and fluxes of $^{12}CO_2$ and $^{13}CO_2$. For a reservoir *x* with a carbon isotopic ratio of $\delta^{13}C_x$

$$\mathbf{R_x = (\delta^{13}C_x\ R_{std}) / 1000 + R_{std}} \quad (14)$$

$$\mathbf{^{13}C = (R_x\ C_x) / (1 + R_x)} \quad (15)$$

$$\mathbf{^{12}C = C_x / (1 + R_x)} \quad (16)$$

where R_x is the $^{13}C/^{12}C$ ratio of the reservoir, R_{std} is the $^{13}C/^{12}C$ ratio of the standard (Pee Dee Belemnite), and C_x is the concentration of CO_2 is reservoir *x*. We handle fluxes (F_x) the same way, except that the $\delta^{13}C_x$ of the flux is a function of both the carbon isotopic ratio of the source as well as isotopic discrimination associated with the reaction. For example, we calculate $^{13}C/^{12}C$ ratios of isotopically fractionated fluxes due to C3 photosynthesis as follows.

$$\mathbf{R_{C3} = R_{ca} / [(\Delta_{C3} /1000) + 1]} \quad (17)$$

Where R_{ca} and R_{C3} are the $^{13}C/^{12}C$ ratios of canopy CO_2 and carbon assimilated by C3 plants, respectively. Individual ^{13}C and ^{12}C fluxes are then

$$\mathbf{^{12}C_{C3} = An_{C3} /(1 + R_{C3})} \text{ and} \quad (18)$$

$$\mathbf{^{13}C_{C3} = R_{C3}\ An_{C3}/(1 + R_{C3})}. \quad (19)$$

Concentrations, fluxes and carbon isotopic ratios CO_2 are calculated each 10-minute time step.

Biotic Isotopic Disequilibrium.

Soil organic matter is older than living biomass and consequently, $\delta^{13}C$ of respired soil carbon is slightly enriched in ^{13}C relative to living plant biomass (Fig. 4). This correction is referred to as the Biotic Isotope Disequilibrium (BID) and is the Suess Effect applied to the

terrestrial environment [Cias et al., 1999]. Since fossil fuels are isotopically light relative to atmospheric CO_2, $\delta^{13}C$ of atmospheric CO_2 has decreased over time due to the continued influx of isotopically depleted fossil fuels. As a result, a significant fraction of soil organic matter formed under an atmosphere in which $\delta^{13}C$ of atmospheric CO_2 was enriched in ^{13}C relative to CO_2 of the present atmosphere. The biotic isotopic disequilibrium is equal to the difference in $\delta^{13}C$ of atmospheric CO_2 in the year of the simulation (1987) and the 'year' that the soil carbon was assimilated, i.e. 1987 minus the flux-weighted age of respired carbon ($\delta^{13}C_{SOM}$).

$$\Delta\delta^{13}C_{BID} = \delta^{13}C_{SOM} - \delta^{13}C_{1987}$$

$\delta^{13}C$ values of atmospheric CO_2 are from Francey et al., [1999]. $\delta^{13}C$ of atmospheric CO_2 for 1987 from this record is –7.70‰. The flux-weighted age of soil carbon is calculated in the CASA model. The amount of the enrichment due to biotic isotope disequilibrium varies zonally, reflecting patterns in the flux-weighted age of respired CO_2. In general, the correction is greatest at high latitudes (~0.65‰), where turnover rates of soil organic carbon are slowest, and near the equator (~0.50‰), where soil carbon is dominated by less easily metabolized woody fractions.

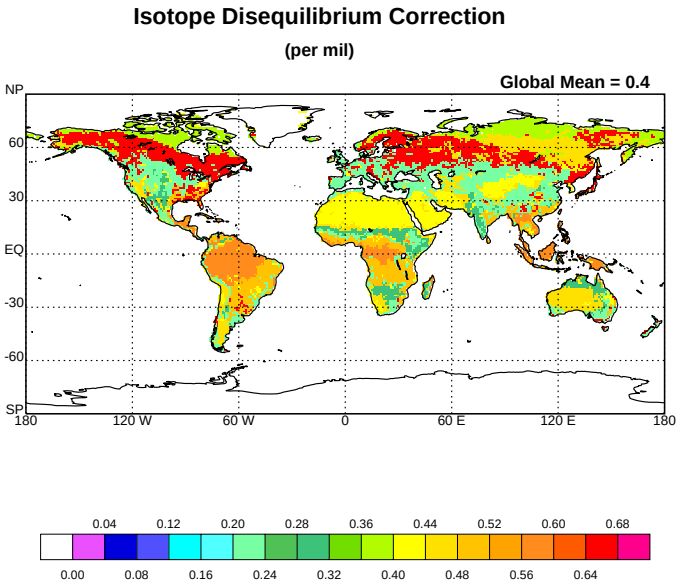

Figure 4. Biotic isotopic disequilibrium. Indicates offset between $\delta^{13}C$ of living plant biomass and respired soil CO_2. Units are per mil (‰).

Terrestrial Biosphere Fluxes

Monthly mean rates of $^{12}CO_2$ and $^{13}CO_2$ exchange between the atmosphere and the terrestrial biosphere are computed for a 1° X 1° grid from rates of respiration and photosynthesis, combined with the $\delta^{13}C$ of respiration, and the net isotopic discrimination accompanying photosynthesis. In the model, terrestrial biosphere CO_2 fluxes are in balance when averaged over the entire year. Consequently, the terrestrial biosphere is neither a sink nor a source for atmospheric CO_2. Total net assimilation and respiration are equal to 150 Gt C/year. Since terrestrial fluxes are the result of the difference between respiration and photosynthesis, the spatial and temporal distribution of these fluxes is quite complex (Figs. 5a and b). Perhaps the most dominant feature in the seasonal cycle of terrestrial fluxes is the shift in the boreal forest from being a moderate source for CO_2 during the northern hemisphere winter to being a major sink during the summer. There is also a seasonal cycle in the discrimination factor during photosynthesis (Fig. 6). For example, in the northern boreal forests, the magnitude of photosynthetic discrimination against ^{13}C increases 2 to 4 per mil between May and September, while decreasing a similar amount in the Pampas region of South America.

Oceanic CO_2 Exchange with the Atmosphere

Annual mean air-sea CO_2 fluxes (Fig. 7) are computed in a 4° version of the Princeton Ocean Biogeochemical Model (OBM). The connection between atmospheric CO_2 and oceanic carbon is via gas exchange, which is controlled by the difference in CO_2 partial pressure between the atmosphere and ocean and the gas transfer coefficient. Transfer of $^{13}CO_2$ is corrected for kinetic isotope fractionation effects. Tracers in the OBM that affect CO_2 exchange are phosphate, dissolved inorganic carbon (DIC), $\delta^{13}C$ of DIC, labile dissolved organic carbon (LDOC), $\delta^{13}C$ of LDOC and total alkalinity. An anthropogenic transient pulse of CO_2 and $^{13}CO_2$ is allowed to invade an ocean in dynamic equilibrium with a pre-industrial atmosphere. The ocean is a source for CO_2 in the equatorial region (0.68 Gt/year between 15°S and 15°N); and a sink for CO_2 at the higher latitudes (1.17 Gt/year for 15°N to 90°N and 1.77 Gt/year for 15°S to 90°S). Over the total year, the ocean is a sink for 2.26 Gt of Carbon. There is no seasonal variability in the fluxes.

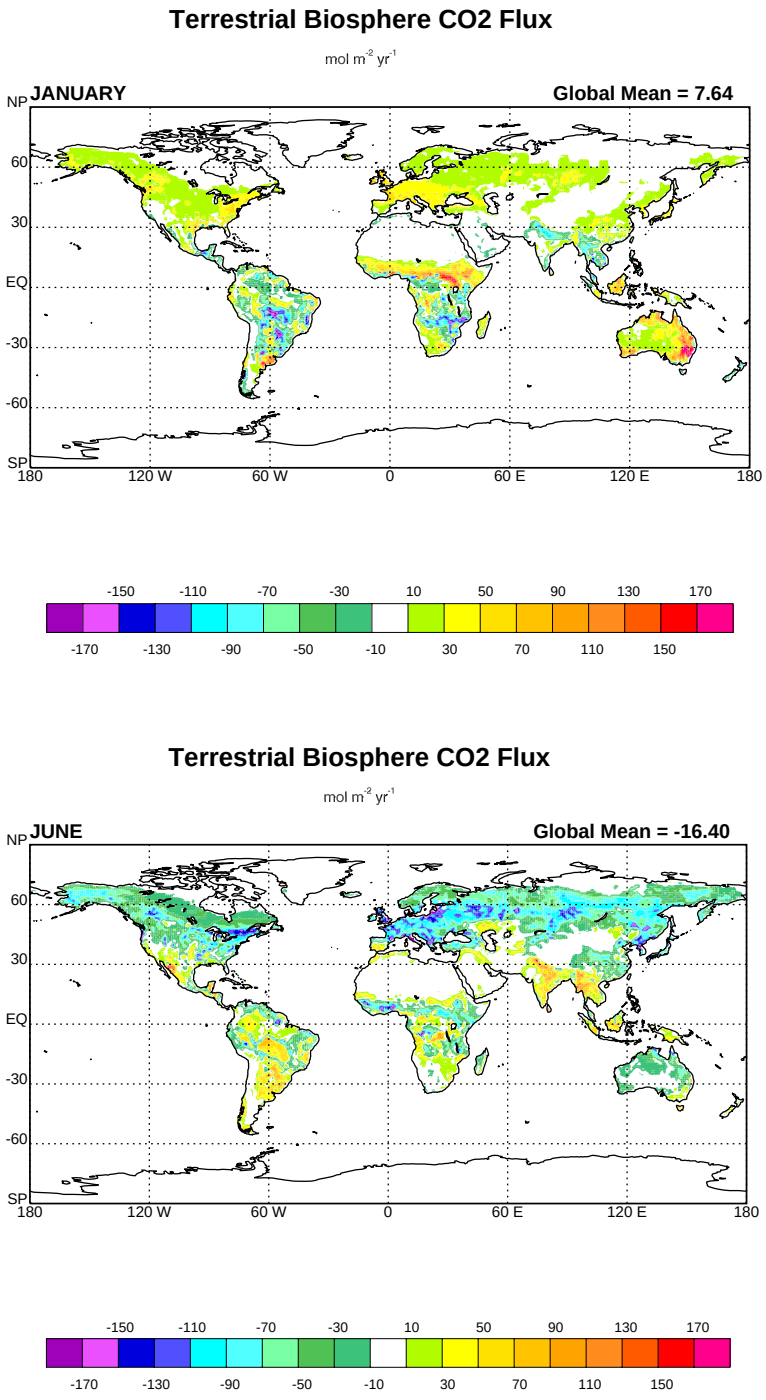

Figures 5a and 5b. CO_2 fluxes from the terrestrial biosphere for the months of (a) January and (b) July. Units are moles per meter squared per year. The large change in fluxes to and from the boreal forests is the most prominent difference between the terrestrial fluxes in these two months. Smaller seasonal cycles in other parts of the globe can also be discerned.

Fossil Fuel CO_2 Fluxes

Anthropogenic CO_2 emissions from fossil fuel combustion and cement manufacture amount to 5.56 Gt-C/year (Fig. 8). They were derived from 1° X 1° data sets for 1990 provided the Carbon Dioxide Information Analysis Center [Andres et al., 1996]. The carbon isotopic ratio of the fluxes is –27.3 (Andres et al., 1994 {to be changed to -28.4 based on Andres et al., 2000). There is no seasonal variability in the modeled fluxes.

Atmospheric transport: TM2 Simulations

In order to test our model, we introduce the predicted CO_2 fluxes to an atmospheric transport model (TM2) and compare simulated concentrations and $\delta^{13}C$ of atmospheric CO_2 to observations of the NOAA Global Flask Network. TM2 uses observed wind fields for 1987 to *advect* terrestrial, oceanic and fossil fuel $^{12}CO_2$ and $^{13}CO_2$ fluxes throughout the globe. We interpolate 1° X 1° terrestrial and fossil fuel fluxes and 4° X 5° ocean fluxes on to an 8° X 10° grid used in TM2. The simulation runs for 4 years in order to ensure complete hemispheric mixing. At the end, January South Pole ^{12}C and ^{13}C concentrations for each tracer are subtracted from each grid cell and a background CO_2 concentration (350ppm @ -7.8‰) is added back in. Monthly concentrations and $\delta^{13}C$ value of terrestrial CO_2, oceanic CO_2, fossil fuel CO_2 and total CO_2 are then calculated in each grid cell. Monthly maps of total CO_2 and $\delta^{13}C$ of total CO_2 are interpolated back to a 1° X ° grid and used as an atmospheric CO_2 boundary condition in further simulations.

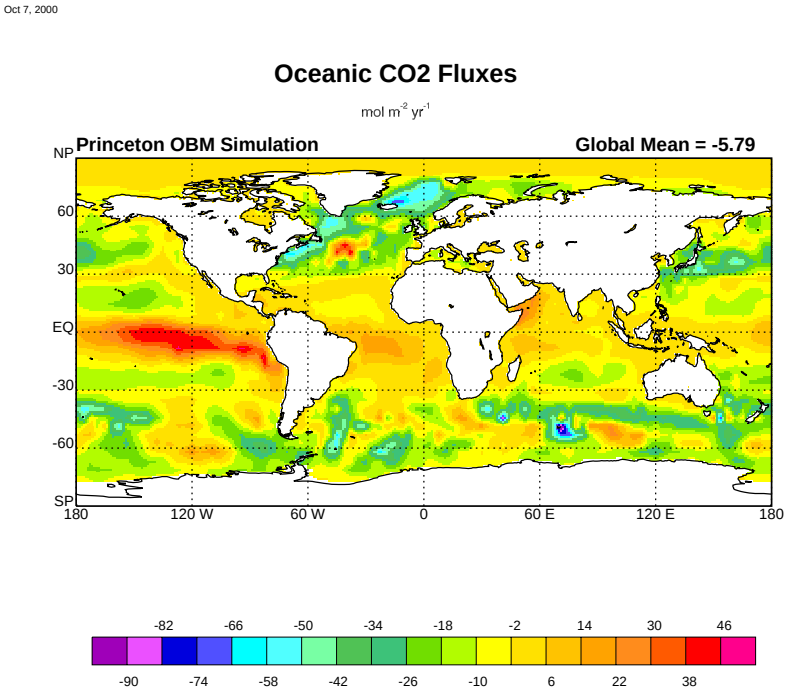

Figure 6. CO_2 exchange between the ocean and atmosphere. Units are moles per square meter per year. The most prominent feature is dominance of CO_2 sinks at the high latitudes and sources for CO_2 near the equator.

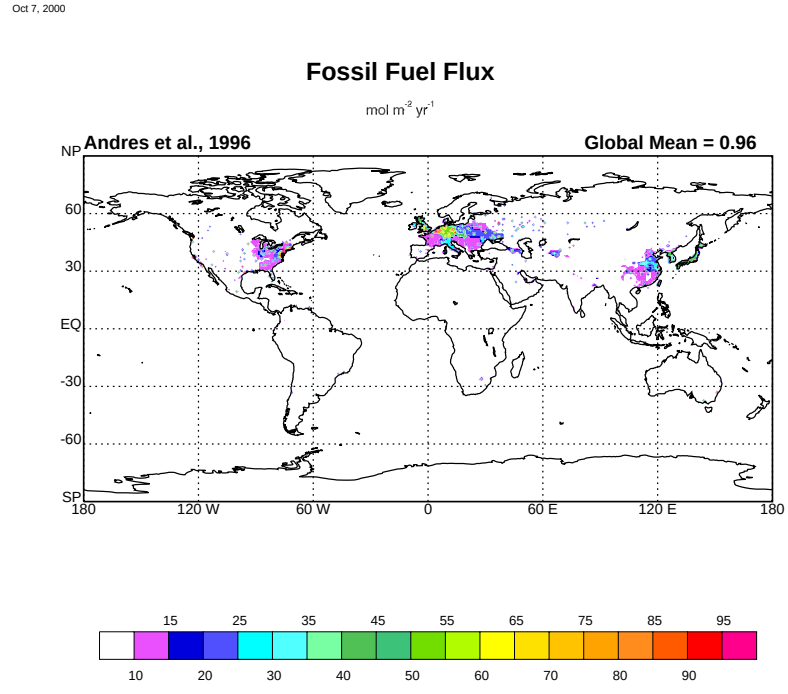

Figure 7. CO_2 fluxes to the atmosphere due the combustion of fossil fuels and manufacture of cement from Andres et al., [1996]. Units are moles per square meter per year. Nearly all of the flux is from the northern industrial population centers. $\delta^{13}C$ of the flux is constant at –27.3‰

Results and Discussion

Carbon isotope discrimination within the terrestrial biosphere

$\delta^{13}C$ of plant carbon

Spatial distribution of $\delta^{13}C$ of plant carbon is quite complex and reflects climate, biome type, C3/C4 distributions, as well as spatial variation in isotopic discrimination during C3 photosynthesis (Fig. 9). Zonal patterns are much clearer. The most pronounced variations are the result of the distribution of C3 and C4 plants. Overlain on this pattern is a zonal trend in isotope discrimination by C3 plants. The heaviest zonally averaged $\delta^{13}C$ values in the terrestrial biosphere (~10 to11‰) are found approximately 10° north and south of the equator, and mirror the distribution of C4 grasslands. $\delta^{13}C$ values are generally most negative at high northern latitudes and reflect the absence of C4 plants, as well as increased discrimination in C3 plants due to zonal variations in the C_{cc}/C_a ratio.

Seasonal variation in isotopic discrimination

There are significant seasonal variations in isotopic discrimination. For example, in the northern boreal forests, mean monthly discrimination decreases by 2 to 4‰ during the growing season, i.e. from May to September. There are similar variations in isotopic discrimination in the tropics, although they are somewhat smaller.

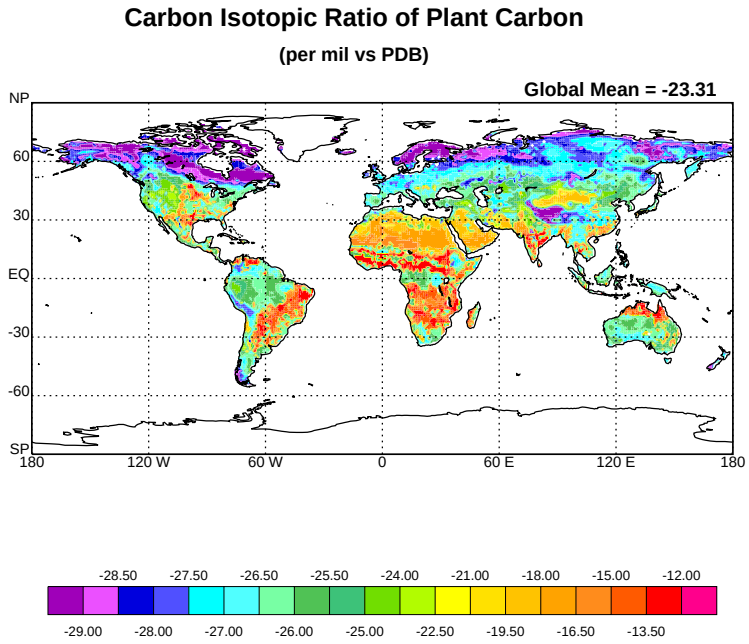

Figure 8. Carbon isotopic ratios of living plant biomass predicted in this simulation. Values are expressed in per mil (‰) versus Pee Dee Belemnite (PDB). The lightest values are found in boreal forests.

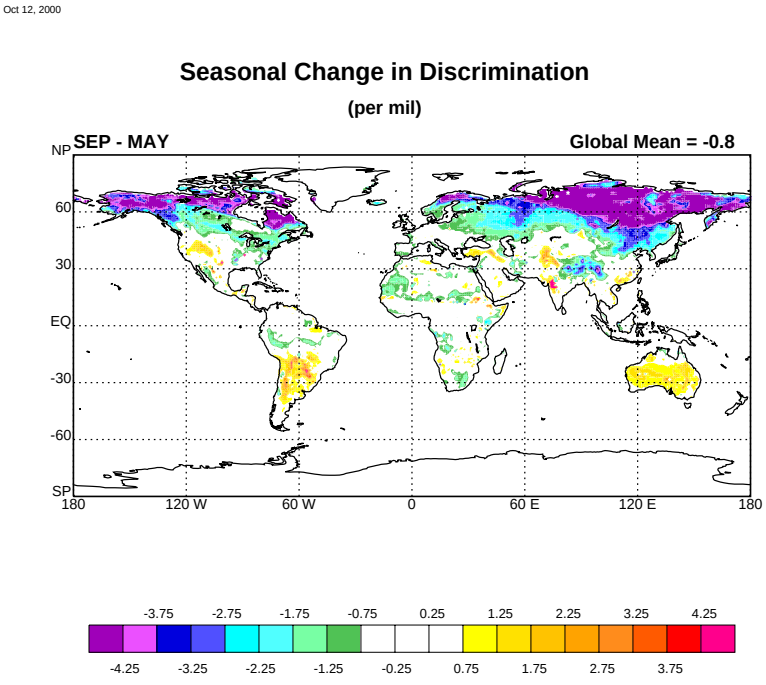

Figure 9. Changes in the carbon isotopic discrimination factor of C3 plants during the growth season in the Northern Hemisphere. Units are per mil (‰). The discrimination factor decreases by 2 to 4‰ in the high northern latitudes between September and May.

Influence of the terrestrial biosphere on atmospheric CO_2

Seasonal variations in $\delta^{13}C$ of atmospheric CO_2

Seasonal variation in $\delta^{13}C$ of atmospheric CO_2 in these simulations is greatest in the Northern Hemisphere at latitudes north of 30° (Figs. 10a and b). The maximum amplitude (2.4‰) is found in the continental areas of western Asia. The signal is produced by influence of the boreal summer-winter cycle on rates of respiration and photosynthesis in the terrestrial biosphere, and is magnified during atmospheric transport over large expanses of continental Eurasia. There is also a seasonal cycle of smaller magnitude in the tropics between South American and African forests. These signals are out of phase and result from seasonal changes in precipitation, zonal C4 plant distributions, as well as shifts in zonal winds and the position of the Intertropical Convergence Zone.

The model successfully simulates seasonal changes in concentration and $\delta^{13}C$ of CO_2 at NOAA Flask sites. The signal is almost completely controlled by fluxes from the terrestrial biosphere (Fig. 11). Ocean-atmosphere exchange and fossil fuel fluxes are smaller factors in determining seasonal variations in either concentration or $\delta^{13}C$ of atmospheric CO_2. Although the fossil fuel and ocean fluxes in the model do not have a seasonal cycle, they do produce a secular trend in $\delta^{13}C$. Fossil fuel combustion causes an annual decrease in $\delta^{13}C$ of CO_2 near Barrow of approximately 0.14‰. Oceanic exchange opposes this effect by of increasing $\delta^{13}C$ of CO_2 by 0.07‰. Total change in $\delta^{13}C$ of Barrow CO_2 in the model is a decline of 0.11‰, whereas the observed decline is only 0.05‰. The difference between these two values largely reflects the fact that we have not included a terrestrial sink in the simulation.

There are two significant differences between the simulated and the observed seasonal cycles in pCO_2 and $\delta^{13}C$. The first is that, in general, the amplitude of the simulated cycle is greater than the observed amplitude (Figs. 12a-l). For example, the amplitude of the observed $\delta^{13}C$ signal at Barrow is 0.81‰, whereas the modeled amplitude is 1.1‰, or nearly 40% greater. In contrast, the amplitude of the observed seasonal variation in CO_2 at Barrow is 14.2 ppm, whereas the modeled amplitude is 20.6 ppm, or approximately 40-45% greater. This indicates that either 1) the terrestrial fluxes are too great, 2) timing of respiration and/or assimilation are incorrectly simulated, 3) timing of the missing sink has an important influence on observed

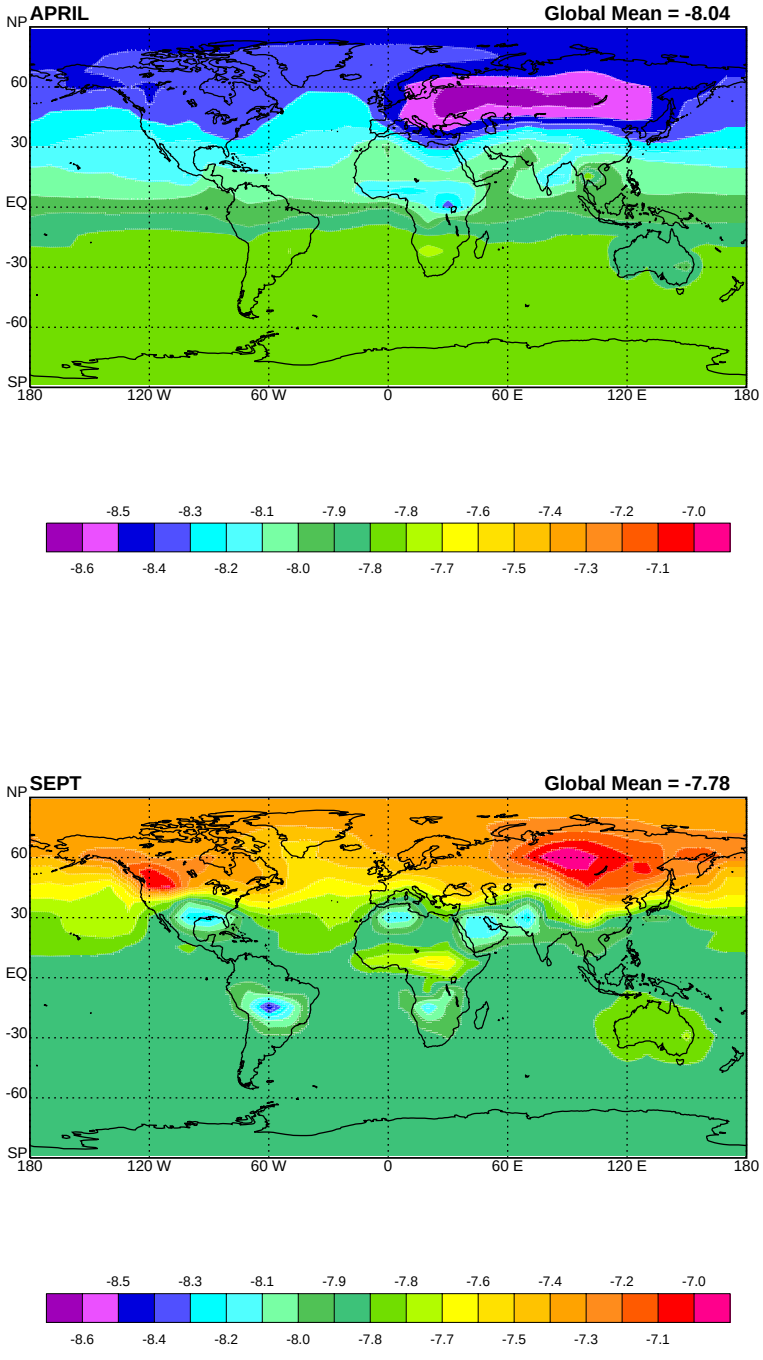

Figure 10. $\delta^{13}C$ of atmospheric CO_2 at the beginning of the Northern Hemisphere growing season, April, (a), and end of growing season, September, (b). The greatest amplitude in the seasonal cycle of $\delta^{13}C$ is observed in continental Asia.

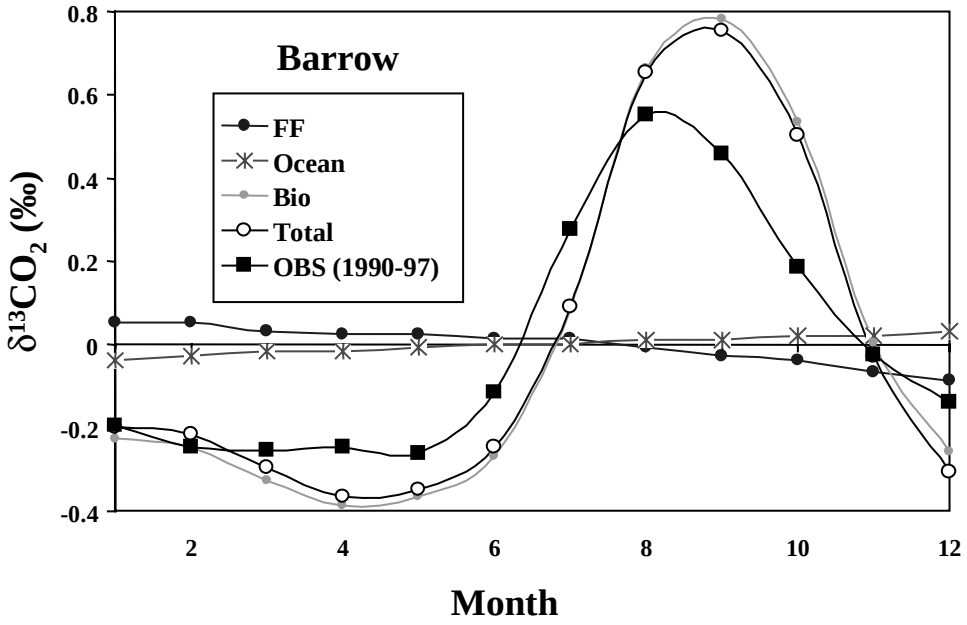

Figure 11. The contributions of CO_2 fluxes from the terrestrial biosphere, oceanic exchange and fossil fuel combustion to seasonal variations in $\delta^{13}C$ of CO_2 at Barrow, Alaska. Units are ‰. Variations are plotted as deviations from the annual mean $\delta^{13}C$. Fluxes from the terrestrial biosphere dominate the seasonal signal. Fossil fuel fluxes cause $\delta^{13}C$ of CO_2 to decrease during the year. Oceanic exchange is a sink for CO_2 and causes $\delta^{13}C$ of CO_2 to increase. In the model, fluxes due to fossil fuel combustion and oceanic exchange are constant throughout the year, and, consequently, deviations from a monotonic signal for these two components are produced by transport processes in TM2.

signals that is not properly represented in the simulations, 4) the influence of the ocean is improperly modeled, or 5) transport has mixed the fluxes improperly.

We believe that one source of error may be that the simulated terrestrial CO_2 fluxes are too great. The fluxes scale linearly with rates of global net assimilation. For 1987, we estimated a Net Assimilation (Net Assimilation = Photosynthesis - Photorespiration - Canopy Autotrophic Respiration) of ~150 Gt-C. Based on the relationship between Net Assimilation and Net Primary Production (NPP), this would indicate that NPP was approximately 70 Gt-C/year [Ryan et al., 1991]. This estimate, though not extreme, is higher than that of many other simulations of terrestrial biosphere [Cramer et al., 1999].

Inaccurate simulation of phase differences between rates of respiration and photosynthesis can also result in overestimating the amplitude of the seasonal cycle. A large phase difference between seasonal variations in rates of respiration and photosynthesis will produce a greater amplitude in seasonal CO_2 cycle because it will reduce in more destructive

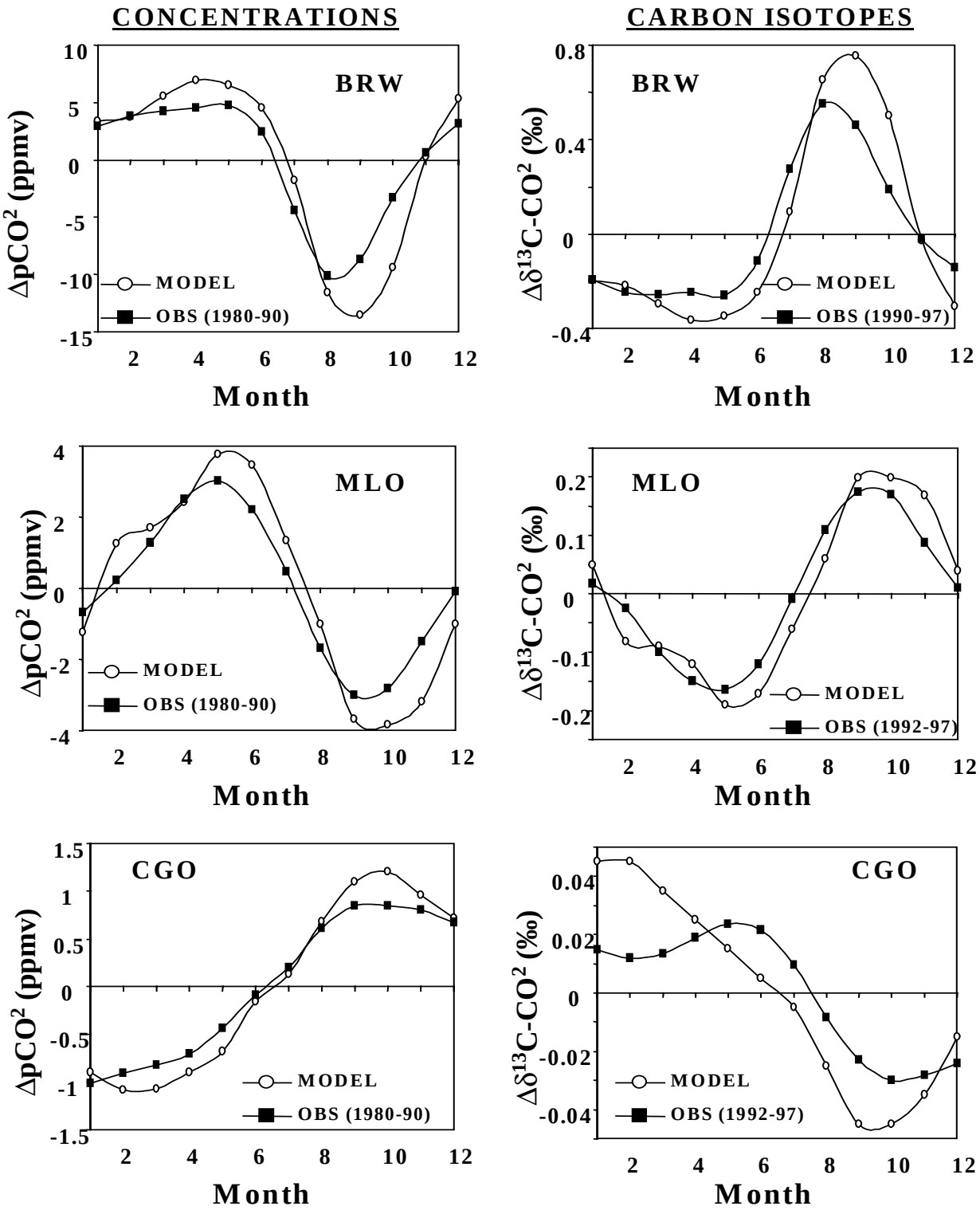

Figures 12a-l. Seasonal variations in concentrations and $\delta^{13}C$ of atmospheric CO_2 at 6 selected sites from the NOAA Global Flask Network. The sites include Barrow, Alaska (BRW), Mauna Loa, Hawaii (MLO), Cape Grim, Australia (CGO), northern Wisconsin (WLEF), Niwot Ridge, Colorado (NWR),

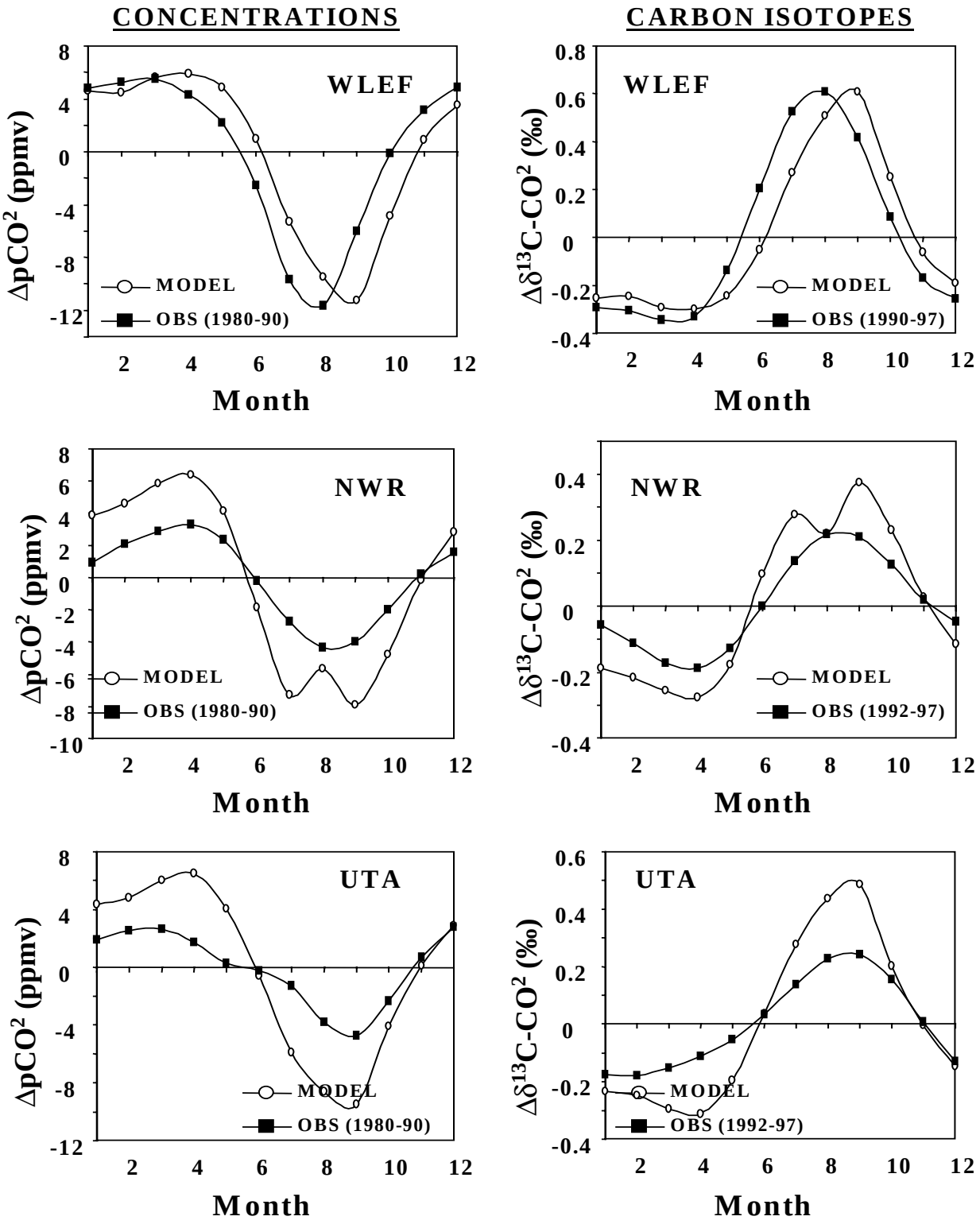

Figures 12 a-l (continued). Wendover, Utah (UTA). Units for CO_2 concentrations are ppmv. Units for $\delta^{13}C$ are per mil. Both are plotted as deviations from the annual mean at that site. Averaged observed values for the time period specified on the graph are plotted as solid squares. Simulated values are the open circles.

interference in their signals. SiB2 uses NDVI to determine the onsite of photosynthesis in the spring, and, consequently should be relative accurate. In contrast, there is no is not external verification for rates of respiration. Consequently, respiration is a complex function of soil moisture and temperature. These, in turn, are sensitive to simulations of seasonal transitions in snow cover and soil dynamics, which can be difficult to attain.

The situation is further complicated by the fact that the amount that the amplitude is overestimated varies from one site to the next. For instance, at WLEF (12g and h) the amplitudes of the simulated and observed cycles are almost identical. This may be caused by the fact that some sites such as Barrow (BRW) integrate isotopes and fluxes over a large area, whereas WLEF tends to reflect more local processes. Other possibilities include improper transport as simulated by TM2.

The second major difference between simulated and observed cycles of pCO_2 and $\delta^{13}C$ is that the simulated signal leads the observed signal by between a half to a full month, depending on the location. This also suggests that there may be discrepancies between phases of simulated and observed rates of respiration and photosynthesis. However, it could also indicate problems with either transport.

Keeling plots, constructed from CO_2 and $\delta^{13}C$ measurements at the NOAA Flask sites, can provide insight into the nature of isotope exchange [Keeling, 1958]. In a linear regression of $1/CO_2$ vs $\delta^{13}C$ of CO_2, the y-intercept represents the $\delta^{13}C$ ratio of the source ($\delta^{13}C_{SRC}$). The correlation coefficient (R^2) can also be informative. In cases where there are multiple sources and sinks for CO_2, each with a distinct $\delta^{13}C$ ratio, the $\delta^{13}C$ ratio of the y-intercept is approximately a flux-weighted mean of the sources, whereas R^2 indicates the degree to which changes in the fluxes and transport from the sources co-vary in a coherent manner. In our simulation, $\delta^{13}C_{SRC}$ is consistently depleted in ^{13}C compared to the observations (Fig. 13). The difference ranges from 2‰ in northern latitudes greater than 30°N, to 8-10‰ in the Southern Hemisphere. This discrepancy can be caused by several different means. First, estimated $\delta^{13}C$ ratios of plant carbon for the terrestrial biosphere could be too low. Second, $\delta^{13}C$ estimates for oceanic exchange and/or fossil fuel fluxes in the simulation could be too light. And third, although atmospheric transport cannot fractionate isotopes, seasonal changes in wind direction

can cause real changes in $\delta^{13}C_{SRC}$. TM2 has a lower resolution that any of the flux fields: 8 X 10 for TM2, 4 X 5 for ocean fluxes, and 1 X 1 for the terrestrial biosphere and fossil fuel. We think that the offset largely reflects the fact that there is no 'seasonality' in either oceanic and fossil fuel fluxes within the model. Consequently, the total natural variation in these fluxes is not captured in the simulation and is therefore not reflected in the calculation of $\delta^{13}C_{SRC}$.

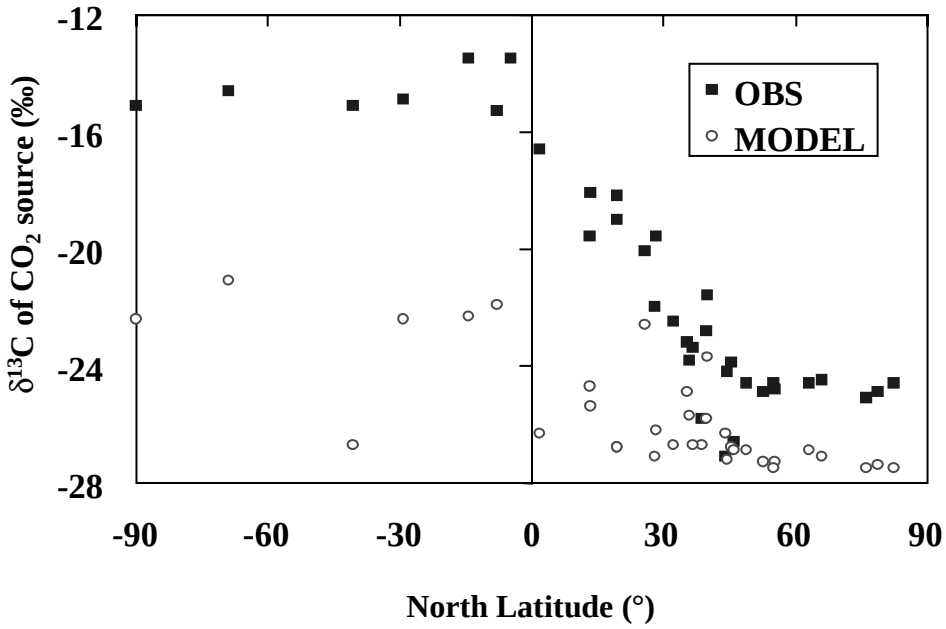

Figure 13. A comparison between Keeling plots from simulated and observed variations in p CO_2 and $\delta^{13}C$ of atmospheric CO_2 at sites from the NOAS Global Flask Network. Simulated $\delta^{13}C_{SRC}$ is systematically depleted in $\delta^{13}C$ relative observed $\delta^{13}C_{SRC}$.

Influence of $\delta^{13}C$ of atmospheric CO_2 on $\delta^{13}C$ of the terrestrial biosphere

Influence of a seasonal atmosphere on $\delta^{13}C$ of plant carbon

We compare results of two simulations: one in which seasonal variations in $\delta^{13}C$ of atmospheric CO_2 calculated in TM2 are used as a boundary condition, and another where $\delta^{13}C$ of atmospheric CO_2 is spatially and temporally constant, in order to look at the influence on seasonal variations in $\delta^{13}C$ of CO_2 on carbon isotopic ratios of plant biomass. The model indicates that interaction between the atmosphere and the terrestrial biosphere enriches $\delta^{13}C$ values of plant carbon over a large region in western Asia and the coastal northwest of North

America, while depleting it in the southeast US and north Africa (Fig. 14). These changes are a function of the timing of the growth season in a specific region relative to seasonal variations in $\delta^{13}C$ of atmospheric CO_2 in that region, and, in particular, to the nature of CO_2 exchange between the atmosphere and earth's surface in the upwind direction. For example, $\delta^{13}C$ of plant carbon is enriched by up to 0.7‰ in continental Asia because the air that feeds this region has passed over large stretches of the terrestrial ecosystem that are both highly productive, and highly seasonal. In the NW coast of North America, the enrichment may indicate that 1) the area is within the 'Asian plume' of ^{13}C depleted CO_2, and 2) that it has not been significantly altered during its passage over the north Pacific because there is little ocean-atmosphere exchange in the region of the ocean. In contrast, $\delta^{13}C$ of plant carbon in the southeastern USA is slightly depleted because the air masses feeding this area have generally passed over the ocean. Two other factors may contribute to depletion of ^{13}C in plant carbon in the Southeast US and North Africa. The first is that growth in these dry areas is often concentrated in the early part of the growing season, before $\delta^{13}C$ of the CO_2 in the atmosphere has begun to rise. Dry conditions later in the season can cause growth to slow, or even cease, just when $\delta^{13}C$ of atmospheric CO_2 is at a maximum. Dry conditions can also favor a temporary increase in local rates of respiration. Second, isotopic depletion of plant carbon in these areas also occurs because of their vicinity to the major sources of fossil fuel CO_2. CO_2 in the atmosphere over the southeastern US and North Africa is depleted in ^{13}C in part due to the influx of air rich in CO_2 from fossil fuel combustion. In the Midwest and Northeast US, the 'continentality' of the air masses over this region overwhelms the fossil fuel signature. In contrast, in the southeast, the continental signal is too weak. Nevertheless, the major effect of interaction between the terrestrial biosphere and the atmosphere is to enrich $\delta^{13}C$ values of plant carbon. This is because not only are the areas where $\delta^{13}C$ of biomass is enriched much large than the areas where it is depleted, they are also much more vigorous ecosystems.

Since these interactions between the atmosphere and biosphere are controlled by meteorology, it is possible that this mechanism, through changes in weather from year to year, could contribute to interannual fluctuations in the carbon isotopic signature of terrestrial CO_2 fluxes. If the spatial pattern of enrichment in $\delta^{13}C$ of plant carbon remains unchanged from year to year, there is no impact on atmospheric CO_2, because the $\delta^{13}C$ of plant carbon simply assumes

Nov 1, 2000

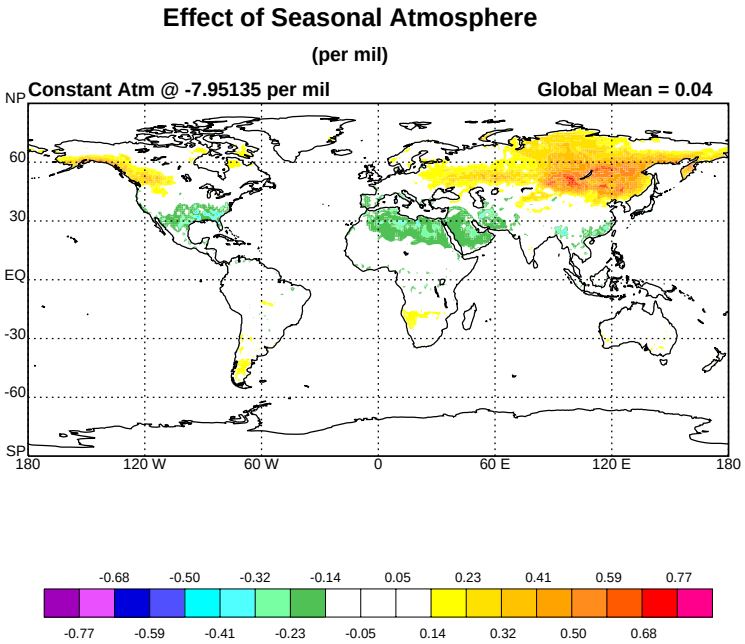

Figure 14. The effect of seasonal variations in $\delta^{13}C$ of atmospheric CO_2 on $\delta^{13}C$ of living plant carbon. $\delta^{13}C$ of plant carbon is enriched in ^{13}C in western Eurasia and depleted in the southern United States and northern Africa.

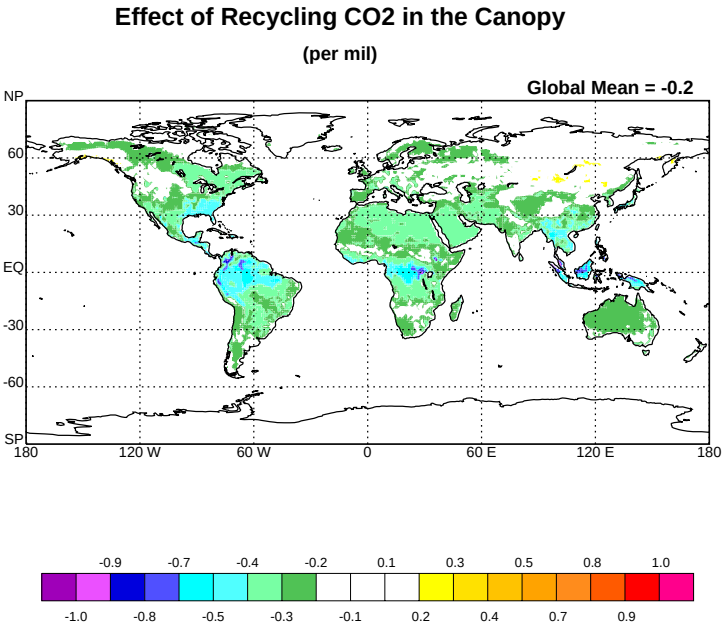

Figure 15. The effect of CO_2 recycling within the canopy on $\delta^{13}C$ of living plant carbon. In general, recycling of isotopically de3pleted, respired CO_2 causes $\delta^{13}C$ of plant carbon to become depelted in ^{13}C.

a 'enriched' steady state value. On the other hand, if changes in weather result in changes in the spatial distribution of primary production and/or transport, it could alter the carbon isotopic signature of the fluxes, and thereby affect $\delta^{13}C$ of atmospheric CO_2. However, the effect could act as a negative feedback on interannual changes in $\delta^{13}C$ of CO_2, because this specific mechanism decreases discrimination of the terrestrial ecosystem, at least in some areas of the globe. The effect could also be bolstered by the fact that, all other things equal, the photosynthetic discrimination is generally lower at higher rates of assimilation. In other words, the flux of CO_2 and $\delta^{13}C$ of the CO_2 are inversely correlated resulting in a negative feedback on changes in $\delta^{13}C$ of CO_2 fluxes from the terrestrial biosphere.

Influence of recycling of canopy CO_2 on $\delta^{13}C$ of plant carbon

In contrast, recycling CO_2 in the canopy, i.e. photoassimilation of respired CO_2, depletes $\delta^{13}C$ of plant carbon by 0.2‰ to 0.8‰ over much of the globe. The effect is greatest in the tropical forests where high rates of respiration and sluggish mixing between the canopy and overlying atmosphere result in significant rates of CO_2 reassimilation. The amount of recycling that actually occurs is in some dispute. Based on measurements of concentration and $\delta^{13}C$ of CO_2 in the canopy, estimates as high as 30% have been made [Sternberg et al., 1996 and references therein]. However, this analysis has been disputed by Lloyd et alia [1996], who argue that the amount of recycling is less than 1%. We can use the isotopic offset to estimate the percentage of respired CO_2 that is recycled. If all of the assimilated CO_2 was from respiration, the $\delta^{13}C$ value of the plant carbon would be equal to the discrimination plus the $\delta^{13}C$ of the SOM, which is approximately equal to the discrimination plus the $\delta^{13}C$ of the atmosphere. On the other hand, if all of the assimilated carbon came from the atmosphere, the $\delta^{13}C$ of the SOM would be the discrimination plus the $\delta^{13}C$ of the atmosphere. In other words, the isotopic offset due to recycling divided by the discrimination is a measure of the amount of CO_2 that has been recycled. Therefore, model results indicate that in tropical forests, approximately 4% of the CO2 is reassimilated before it can escape the canopy. These estimates, however, only pertain to recycling of canopy CO_2. They do not include assimilation of respired CO_2 that has entered the boundary layer, only to be mixed back down into the canopy at a later time. Consequently, this estimate of the percent recycled should be considered a bottom limit. Although the model has a

diurnal cycle in concentration and $\delta^{13}C$ of canopy CO_2, it does not interact with TM2 on a diurnal basis. Consequently, there is no 'rectification' of the day/night CO_2 fluxes.

Recycling canopy CO_2 could affect the carbon isotopic signature of the fluxes in two ways. First, it could affect interannual variations in $\delta^{13}C$ of terrestrial fluxes. The nature and magnitude of the effect depends on the relationship between climatology and rates of photosynthesis, respiration and recycling. For instance, at moderate levels, precipitation enhances both respiration and photosynthesis. As the amount of rain increases, soils become waterlogged and respiration rates decline. In general, however, conditions favorable for plant growth also favor higher rates of respiration. They will probably produce a denser canopy as well. Since the latter tends to cause a decrease in turbulence in the canopy, it should also result in greater rates of recycling. Consequently, a vigorous growth season should increase recycling, and thus cause an increase in the carbon isotopic signal to the atmosphere because it would increase both rates of assimilation as well as the net discrimination of the terrestrial biosphere. Second, recycling CO_2 could alter the diurnal signal of CO_2 from the canopy. Most recycling occurs during photosynthesis in the early morning, before ^{13}C-depleted CO_2 that has accumulated during the previous night has time to be flushed from the canopy. Carbon isotopic discrimination during assimilation would tend to enrich the early morning flux relative to what one might expect based on Keeling plots within the canopy. Consequently, systematic interactions between carbon isotopic discrimination, canopy dynamics and seasonal variations in global mixing could affect the expression of net carbon isotopic discrimination of terrestrial ecosystems.

Conclusion

We use an ecophysiological model of the terrestrial ecosystem (SiB2), driven by observed meteorology provided by the European Center for Medium-range Weather Forecasts (ECMWF), and coupled offline to an atmospheric tracer-transport model (TM2), to generate seasonally and spatially varying concentrations and carbon isotope ratios of atmospheric carbon dioxide. Terrestrial $^{12}CO_2$ and $^{13}CO_2$ fluxes from SiB2 are then combined with similar fluxes

produced by 1) fossil fuel burning and 2) exchange with the ocean as calculated in an ocean biogeochemical model. These total fluxes are prescribed to TM2 in order to predict seasonal and spatial variations in carbon isotope ratios of atmospheric CO_2, which are then compared to measurements from the Global Flask network. Predicted seasonal cycles of concentrations and carbon isotope ratios of CO_2 compare well with observations, although there are slight discrepancies in both magnitude and phase of these two parameters. A comparison of results of Keeling plots from the simulation and from data collected at sites from the NOAA Global Flask Network show that the simulation systematically underestimates $\delta^{13}C$ values of CO_2 contributing to variations in p CO_2 and $\delta^{13}C$ at these sites. Results indicate that seasonality in $\delta^{13}C$ of atmospheric CO_2 tends to enrich carbon isotopic ratios of living plant carbon over large areas of western continental Eurasia, while depleting it in the southern United States and northern Africa. Results further indicate that recycling of respired CO_2 in the canopy depletes carbon isotope ratios of plant carbon by a few tenths of a per mil (‰).

Acknowledgements

Martin Heimann: TM2; Inez Fung: Discussions; NOAA-CMDL Data; NSF Grant #ATM-9896261.

References

Andres, R.J., Marland, G., Boden, T. and Bischof, S. Carbon dioxide emissions from fossil fuel consumption and cement manufacture, 1751-1991, and an estimate of their isotopic composition and latitudinal distribution. In: Wigley, T. and Schimel, D. (eds.) Global Change Institute, Cambridge University Press, Oxford. 1996.

Ball, M.C., Cowan, I.R. and Farquhar, G.D., Maintenance of leaf temperature and the optimization of carbon gain in relation to water loss in a tropical mangrove forest. *Aust. J. Plant Physiol.*, 15, 263-276. 1988.

Berry, J.A., Studies of mechanisms affecting the fractionation of carbon isotopes in photosynthesis, In: Stable Isotopes in Ecological Research, Rundel, P.W. et al. (eds.) 82-94, 1988.

Bousquet, P, Ciais, P, Peylin, P., Ramonet, M., and P. Monfray, Inverse modeling of annual atmospheric CO_2 sources and sinks. Part 1: method and control inversion, *J. Geophys. Res*, 104 (D21) 26161-26178, 1999a.

Bousquet, P, Ciais, P, Peylin, P., Ramonet, M., and P. Monfray, Inverse modeling of annual atmospheric CO_2 sources and sinks. Part 2: sensitivity study, *J. Geophys. Res*, 104 (D21) 26179-26193, 1999b.

Ciais, P., Tans, P.P., Trolier, M., White, J.W.C. and R. J. Francey, A large northern hemisphere terrestrial sink induced by the ^{13}C /^{12}C ratio of atmospheric CO_2, *Science*, *269*, 1098-1102, 1995a.

Ciais, P. Tans, P.P., White, J.W.C., Trolier, M., Francey, R.J., Berry, J.A., Randall, D.R., Sellers, P.J., Collatz, J.G. and D.S. Schimel, Partitioning of ocean and land uptake of CO_2 as inferred by $\delta^{13}C$ measurements from the NOAA Climate Monitoring and Diagnostics Laboratory Global Air Sampling Network, *J. Geophys. Res., 100*, 5051-5070, 1995b.

Collatz, G. J., Ball, J. T., Grivet, C. and J. A. Berry, Physiological and environmental regulation of stomatal conductance, photosynthesis, and transpiration: a model that includes a laminar boundary layer, *Agric. and Forest Meteorol*., *54*, 107-136, 1991.

Collatz, G. J., Ribas-Carbo, M. and J. A. Berry, Coupled photosynthesis-stomatal conductance model for leaves of C4 plants, *Aust. J. Plant Physiol*., *19*, 519-538, 1992.

Collatz, G.J., Berry JA. and J.S. Clark, Effects of climate and atmospheric CO_2 partial pressure on the global distribution of C-4 grasses: present, past, and future, *Oecologia, 114*, 441-454, 1998.

Craig, H., The geochemistry of stable carbon isotopes, *Geochim. Cosmochim. Acta, 3*, 53-92, 1953.

Cramer, W., Kicklighter, D.W., Bondeau, Moore, B. III, Churkina, G., Nemry, B., Ruimy, A., Schloss, A.L., and The Participants of the Potsdam NPP Model Comparison. Coparing global models of terrestrial net primary productivity (NPP): overview and key results. *Global Change Biol*., 5, 1-15. 1999.

DeFries, R.S., Townshend, J.R.G. and M.C. Hansen, Continuous fields of vegetation characteristics at the global scale at 1-km resolution. *J. Geophys. Res.-Atmos., 104*,16911-16923, 1999.

Deines, P., The isotopic composition of reduced organic carbon. In: Fritz, P. and Fontes, F.C. (eds.) Handbook of Environmental Isotope Geochemistry. Elsevier, Amsterdam, 329-406. 1980.

Denning, A.S., Fung, I.Y. and Randall, D., Latitudinal gradient of atmospheric CO_2 due seasonal exchange with land biota. *Nature*, 376, 240-243, 1995.

Denning, A. S., Collatz, J. G., Zhang, C., Randall, D. A., Berry, J. A., Sellers, P. J., Colello, G. D. and D. A. Dazlich, Simulations of terrestrial carbon metabolism and atmospheric CO_2 in a general circulation model. Part 1: Surface carbon fluxes. *Tellus, 48B*, 521-542, 1996a.

Denning, A. S., Randall, D. A., Collatz, G. J. and P. J. Sellers, Simulations of terrestrial carbon metabolism and atmospheric CO_2 in a general circulation model. Part 2: Spatial and temporal variations of atmospheric CO_2. *Tellus, 48B*, 543-567, 1996b.

Denning, A. S., Dazlich, D. A. and D. A. Randall, Simulations of soil temperature, snowpack, and carbon fluxes with an atmospheric general circulation model. Presented at 1996 Fall Meeting of the American Geophysical Union A32D-2, 1996c.

Enting, I.G., Trudinger, C.M., and R.J. Francey, A synthesis inversion of the concentration and $\delta^{13}C$ of atmospheric CO_2, *Tellus, 47B*, 35-52, 1995.

Fan, S., Gloor, M., Mahlman, J., Pacala, S., Sarmiento, J., Takahashi, T. and P. Tans,. A large terrestrial carbon sink in North America implied by atmospheric and oceanic carbon dioxide data and models. *Science, 282*, 442-446, 1998.

Farquhar, G. D., von Caemmerer, S. and J. A. Berry, A biochemical model of photosynthetic CO_2 assimilation in C_3 plants, *Planta, 149*, 78-90, 1980.

Farquhar, G.D., On the nature of carbon isotope discrimination in C4 species. *Aust. J. Plant Physiol., 10,* 205-226, 1983.

Farquhar, G.D., O'Leary, M.H. and J.A. Berry, On the relationship between carbon isotope discrimination and the intercellular carbon dioxide concentration in leaves, *Aust. J. Plant Physiol., 9,*121-137, 1982.

Farquhar, G.D., Hubick, K.T., Condon, A.G. and Richards, R.A., Carbon isotope discrimination and plant water use efficiency. In: Stable Isotopes in Ecological Research, Rundel, P.W. et al. (eds.) 21-40. 1988.

Francey, R.J., Allison, C.E., Etheridge, D.M., Trudinger, C.M., Enting, I.G., Leuenberger, M., Langenfelds, R.L., Michel, E. and Steele, L.P., A 1000-year high precision record of $\delta^{13}C$ in atmospheric CO_2. *Tellus,* 51B, 170-193. 1999.

Fung, I., Berry, J. A., Field, C., Thompson, M., Randerson, J., Malmstrom, C., Vitousek, P., Collatz, J., Sellers, P. J., Randall, D. A., Denning, A. S., Badeck, F., and J. John, Carbon-13 exchanges between the atmosphere and biosphere. *Global Biogeochemical Cycles, 11,* 507-533, 1997.

Keeling, C.D., The concentration and isotopic abundances of atmospheric carbon dioxide in rural areas, *Geochim. Cosmochim. Acta, 13,* 322-334, 1958.

Los, S.O., Collatz, G.J., Sellers, P.J., Malmström, C.M., Pollack, N.H., DeFries, R.S., Tucker, C.J., Bounuoa, L and D.A. Dazlich, A global 9-year biophysical landsurface dataset from NOAA AVHRR data, *Geophys Res.,* submitted.

Lloyd, J. and Farquhar, G.D., ^{13}C discrimination during CO_2 assimilation by the terrestrial biosphere. *Oecolgia*, 99, 201-215. 1994.

Mook, W.G., Bommerson, J.G., and W.H. Staverman, Carbon isotope fractionation between dissolved bicarbonate and gaseous carbon dioxide, *Earth Plan. Sci. Let., 22,* 169-176, 1974.

O'Leary, M.H., Measurement of the isotopic fractionation associated with diffusion of carbon dioxide in aqueous solution, *J. Phys. Chem., 88,* 823-825, 1984.

Randall, D.A., Dazlich, D.A., Zhang, C., Denning, A.S.,Sellers, P.J., Tucker, C.J., Bounoua, L., Berry, J.A., Collatz, G.J. Field, C.B., Los, S.O., Justice, C.O. and Fung, I., A revised land surface parameterization (SiB2) for GCMs. Part III. The greening of the Colorado State University general circulation model. *Jour. Of Climate,* 9, 738-763, 1996.

Rayner, P.J., Enting, I.G., Francey, R.J and Langenfelds, R., Reconstructing the recent carbon cycle from atmospheric CO_2, $\delta^{13}C$ and O_2/N_2 observations. *Tellus,* 51B, 213-232. 1999.

Sellers. P.J., Mintz, Y., Sud, Y.C. and A. Dalcher, A simple biosphere model (SiB) for use within general circulation models, *J. Atmos. Sci., 43*, 505-531, 1986.

Sellers, P.J., Shuttleworth, W.J., Dorman, J.L., Dalcher, A. and J.M. Roberts, Calibrating the simple biosphere model for the Amazonian tropical forest using field and remote sensing data. Part I: Average calibration with field data, *J. Appl. Meteor., 28*, 727-759, 1989.

Sellers, P.J., Randall, D.A., Collatz, G.J., Berry, J.A., Field, C.B., Dazlich, D.A., Zhang, C., Collelo, G.D. and L. Bounoua, A revised land surface parameterization (SiB2) for atmospheric GCMs. Part I: Model formulation, *J. Climate, 9*, 676-705, 1996a.

Sellers, P.J., Berry, J.A., Collatz, G.J., Field, C.B. and Hall, F.G., Canopy reflectance, photosynthesis and transpiration. III. A reanalysis using improved leaf models and anew canopy integration scheme. *Remote Sens. Environ.*, 42, 187-216, 1992.

Sellers, P.J., Los, S.O., Tucker, C.J., Justice, C.O., Dazlich, D.A., Collatz, G.J. and D.A. Randall, A revised land surface parameterization (SiB2) for Atmospheric GCMs. Part II: The generation of global fields of terrestrial biophysical parameters from satellite data, *J. Climate, 9*, 706-737, 1996b.

Still, C.J., Berry, J.A., Collatz, G.J. and R.S. DeFries, Global distributions of C4 photosynthesis. In preparation.

Wanninkopf, R., Kinetic fractionation of the carbon isotopes ^{13}C and ^{12}C during transfer of CO2 from the air to seawater. *Tellus*, 37B:128-135. 1985.

Sources and Sinks of Anthropogenic CO_2:

Integrated Assessment Using Biogeochemical Modeling and Inversion of Atmospheric Tracer Transport

Final Report

Jorge Sarmiento, and Song-Miao Fan

Atmospheric & Oceanic Sciences Program, Princeton University

Princeton, New Jersey 08544

Summary: With support from the NSF Methods and Models for Integrated Assessment initiative, we have developed an isotopic method for direct calculation of the sources and sinks of atmospheric CO_2 through inverse modeling of observational data using a GFDL global three-dimensional tracer transport model. We modeled the distribution of $\delta^{13}C$ ratios in the atmosphere observed during 1993-1995, and estimated the terrestrial net ecosystem production for three geographical regions. The land biota in North America and Eurasia was found to be absorbing CO_2, at a rate of about 2 GtC yr^{-1}, while that in Tropics and the Southern Hemisphere were found to be releasing CO_2 during this three-year period.

1. Introduction

The global carbon cycle involves multiple components of the Earth system, including the atmosphere, the ocean, the terrestrial biosphere, and anthropogenic emissions. We proposed an integrated program to develop methods to assess the current carbon budget, and at the same time to build the tools to allow a mechanistic study of the processes involved so that realistic prediction of changes to these processes may become more feasible. In particular, we proposed to develop an isotopic inverse

method for the estimation of terrestrial carbon sources and sinks over the globe as a part of the integrated program.

The following tasks have been completed:

(a) We carried out forward model simulations of carbon isotopes in the atmosphere caused by fossil fuel emissions, annual average air-sea exchange fluxes, and seasonal terrestrial net primary production (NPP) and heterotrophic respiration (RESP).

(b) We developed an isotopic inverse method, and evaluated the inverse method using "synthetic" data generated by a separate atmospheric model. The evaluation provides a critical assessment of transport errors inherent in our inverse estimates.

(c) Terrestrial net carbon fluxes during 1993-1995 were estimated using the inverse method for North America, Eurasia, Tropics and the Southern Hemisphere.

We will document in this report (1) the basics of carbon isotope biogeochemistry, (2) forward modeling of carbon isotopes in the atmosphere using a global chemical transport model, (3) an inverse method for carbon isotopic ratios, and (4) inverse estimates of terrestrial carbon sources and sinks.

2. The Isotopic Method

Measurements of carbon isotopic ratios are often presented in the 'delta notation', $\delta^{13}C$, as follows:

$$\delta^{13}C = \frac{R - R_{PDB}}{R_{PDB}} \times 1000$$

where R is $^{13}C/^{12}C$ ratio, and R_{PDB} = 0.0112372 is the ratio found in Pee Dee Belemnite calcite and the reference ratio used internationally for reporting measurements. Typical values of $\delta^{13}C$ are listed in Table 1 for various carbon reservoirs.

Table 1. Typical isotopic ratios of carbon reservoirs

Carbon reservoirs	$\delta^{13}C$ (‰)
Atmosphere	-6.4 around 1740, -7.8 around 1990
Ocean	~1.6 surface ocean (c. 1990), ~2.1 deep sea
Land biota	-25 for C_3 forests, -12 for C_4 pastures
Fossil fuel	-24 for coal, -44 for natrual gas, -26 to -30 for crude oil
Cement production	0.0
Mean fossil CO_2	-24.1 c. 1860, -28.2 c. 1980, -28.4 c. 1990

We can use the $\delta^{13}C$ ratio of CO_2 to distinguish terrestrial from marine fluxes. Because plants discriminate against ^{13}C in photosynthetic carbon assimilation (see Table 2). By contrast, the kinetic fractionation of carbon isotopes during the transfer from the atmosphere to the ocean is small (-2‰); atmospheric $\delta^{13}C$ is nearly unchanged by the uptake of CO_2 into the surface oceans. The difference of $\delta^{13}C$ between the atmosphere and seawater (~9‰) is mainly due to the kinetic fractionation during the transfer from the ocean back to the atmosphere (-11‰).

The atmosphere is near equilibrium with the surface ocean with regard to the isotopic composition of CO_2. However, a small isotopic dis-equilibrium has resulted from anthropogenic perturbations to the global carbon cycle since the Industrial Revolution. Anthropogenic CO_2 from fossil fuel consumption and deforestation sources is depleted in ^{13}C, causing atmospheric CO_2 and disolved inorganic carbon in seawater to become isotopically lighter (the ratio of $^{13}C/^{12}C$ decreasing) with time. This trend of isotopic ratio is called the "Suess effect". The oceanic Suess effect lags behind

that in the atmosphere due to a relatively long air-sea equilibration time (years) for the isotopic compositions compared to the equilibration time for CO_2 concentrations (months). As a result, an isotopic dis-equilibrium develops between the atmosphere and the global ocean.

Table 2. Typical isotopic fractionation

Processes	*Fractionation* (‰)
Air-C_3 plants	-20
Air-C_4 plants	-4
Air-sea	-2
Sea-air	-10.2

An isotopic dis-equilibrium has similarly developed between soil carbon and atmospheric CO_2, as old soil carbon was assimilated one to hundreds of years ago when the carbon isotopes ratio in the atmosphere was different than at the present time. Because of the presence of the isotopic dis-equilibria, atmospheric $\delta^{13}C$ is changed (increased) even when terrestrial respiration balances terrestrial net primary production and CO_2 evasion from sea to air balances CO_2 invasion from air to sea over annual cycles.

2. Modeling of isotopic ratios

Our goal is to determine the contribution of surface carbon fluxes that will best predict observations of the spatial structure of CO_2 and $\delta^{13}C$ in the atmosphere. We define the spatial structure in reference to South Pole observations (or model results) in **January** of each year, and denote

$$\Delta C = C - C_{SPO} \qquad \text{for } CO_2,$$

$$\Delta^{12}C = {}^{12}C - {}^{12}C_{SPO} \qquad \text{for } {}^{12}CO_2, \text{ and}$$

$$\Delta^{13}C = {}^{13}C - {}^{13}C_{SPO} \qquad \text{for } {}^{13}CO_2.$$

Because the South Pole Observatory (SPO) is remote from carbon sources and sinks, monthly measurements can be obtained from four weekly flask samples with minimal biases due to local and synoptic variations. Local sources represent subgrid variations, and are not resolved in the global model. Changes in the isotopic ratios are given by:

$$\Delta\delta^{13}C = \delta^{13}C - \delta^{13}C_{SPO} = \frac{\Delta R}{R_{PDB}} \times 1000$$

$$\Delta\delta^{13}C = \frac{1000}{R_{PDB}} \Delta\left[\frac{{}^{13}C}{{}^{12}C}\right] = \frac{1000}{R_{PDB}}\left(\frac{\Delta^{13}C}{{}^{12}C} - R_{SPO}\frac{\Delta^{12}C}{{}^{12}C}\right)$$

$$\Delta\delta^{13}C = \frac{1000}{R_{PDB}}\left(\frac{(1+R_{SPO})\Delta^{13}C}{C} - R_{SPO}\frac{\Delta C}{C}\right)(1+R)$$

$$\Delta\delta^{13}C \approx \frac{1000}{R_{PDB}}\left(\frac{(1+R_{SPO})\Delta^{13}C}{C_{SPO}} - R_{SPO}\frac{\Delta C}{C_{SPO}}\right)\left(1-\frac{\Delta C}{C_{SPO}}\right)(1+R)$$

Rearranging above equation, and neglecting the near identity factors (1+R) and (1-$\Delta C/C_{SPO}$), we obtain:

$$C_{SPO} \bullet \Delta\delta^{13}C \approx \frac{1000}{R_{PDB}}\left((1+R_{SPO})\Delta^{13}C - R_{SPO}\Delta C\right)$$

Given surface fluxes of CO_2 and $^{13}CO_2$, we use atmospheric transport models to predict the spatial and temporal structures of ΔC and $\Delta^{13}C$, and then use above equation to compute $\Delta\delta^{13}C$.

We simulated in the GFDL Global Chemical Transport Model (GCTM) atmospheric CO_2 and $\delta^{13}C$ caused by fossil fuel emissions, air-sea exchanges, and seasonal biotic sources and sinks on land. The model specifies fossil fuel emissions based on the estimates of Andres et al. (1995), and prescribes oceanic fluxes based on an aseasonal (annual mean biology) ocean model (Murnane et al., 1998). Figure 1 shows the isotopic ratios of fossil carbon released by each nation. For the United States, we use isotopic ratios estimated for each state and for each month (Figures 2a and 2b), provided to us by Robert Andres at the University of Alaska. Spatial and temporal variations in the isotopic ratios of fossil carbon reflect changes in the types of fuel consumed, with natural gas being the most depleted in ^{13}C and coal the least depleted (see Table 1).

The spatial and temporal patterns for the terrestrial biospheric carbon fluxes are taken from the Carnegie, Ames, and Stanford Approach (CASA) biospheric model (Potter et. al., 1993). The isotopic fractionation coefficients vary significantly from boreal forest to tropical savanna (Neil Suits, Colorado State University). However, we did not have the terrestrial model results when the isotopic inverse model was constructed; we assumed uniform isotopic fractionations for three large regions (Figure 3). It can be shown for a terrestrial source of uniform isotopic ratios that the atmospheric response is given by:

$$C_{SPO}\Delta\delta^{13}C = a(x,t)\left(\delta^{13}C_{leaf} - \delta^{13}C_{SPO}\right)F$$

where *a(x,t)* is atmospheric response at location *x* and at time t to a source of 1 GtC yr^{-1} , and *F* is a flux multiple. Let $\mathbf{D = C_{spo} \bullet \Delta\delta^{13}C}$ (unit: ppm‰). We then have:

where ***i*** = Eurasia, North America, and Tropics+SH, and

$$D_{mod\ el} = D_{fossil} + D_{ocean} + \sum_i (D_{i,resp} - D_{i,npp})$$

$$D_{i,resp} = [iso\_RESP]_i \bullet a_{i,resp}(x,t)$$

$$D_{i,npp} = [iso\_NPP]_i \bullet a_{i,npp}(x,t)$$

The *isotopic fluxes* are related to carbon fluxes by:

$$[iso\_RESP] = (\delta^{13}C_{SOM} - \delta^{13}C_{SPO}) \bullet [RESP] \quad \text{and}$$

$$[iso\_NPP] = (\delta^{13}C_{leaf} - \delta^{13}C_{SPO}) \bullet [NPP]$$

and are in units of ‰GtC yr^{-1} , $a_{i,resp}(\mathbf{x},t)$ and $a_{i,npp}(\mathbf{x},t)$ are predicted CO_2 for CASA model respiration and net primary production (normalized to 1 GtC yr^{-1}), respectively, and are in units of ppm/(GtC yr^{-1})

The inverse model substitutes D_{model} with observations D_{obs}, and then solves

$$D_{obs} = D_{fossil} + D_{ocean} + \sum_i \left(a_{i,resp}(x,t)[iso\_RESP]_i - a_{i,npp}(x,t)[iso\_NPP]_i \right)$$

for the isotopic fluxes [iso_RESP] and [iso_NPP] caused by terrestrial net primary production (NPP) and respiration (RESP) for three land regions: North America (north of 15°N), Eurasia and North Africa (north of 24°N), and Tropics and Southern Hemisphere (Figure 3). We chose to solve for three regions because we are limited by the spatial coverage of observations (Gloor et al., 1999). We used the inverse model to

estimate CO_2 fluxes and isotopic fluxes that give best fit to the the spatial gradients, seasonal variations, and annual trends in atmospheric CO_2 and $\delta^{13}C$ observed at 70 CMDL sampling sites during a three year period between 1993-1995 (Pieter Tans, CMDL; Jim White, University of Colorado INSTAAR). The inverse model uses a robust estimation method that is insensitive to outliers, and uses the "downhill simplex minimization" algorithm (Press et al., 1998).

3. Model Results

Figure 4 shows the distribution of zonal average atmospheric $\delta^{13}C$ caused by fossil emissions and oceanic fluxes. Fossil carbon fluxes cause atmospheric $\delta^{13}C$ to be more negative in the Northern Hemisphere than in the Southern Hemisphere. Oceanic fluxes increase atmospheric $\delta^{13}C$ in the tropics and decrease atmospheric $\delta^{13}C$ in the mid-high latitudes, but do not cause a large north-south gradient.

In order to evaluate the simple inverse model, we used another GFDL atmospheric model (SKYHI) to generate synthetic "data" with the same fossil fuel and oceanic carbon fluxes as used in the GCTM model, and with presumed annual net terrestrial fluxes super-imposed on the CASA model NPP and RESP fluxes. The presumed net terrestrial fluxes are uniformly propotrtional to NPP in each grid cell and in each month. The fluxes estimated by the inversion are shown in Tables 3a-d for four sets of synthetic "data" generated in SKYHI using different presumed fluxes. The global ocean uptake was also estimated in the test inversions, while its spatial distribution was specified. Table 3a shows that the estimated carbon fluxes are close to zero, in good agreement with the presumed fluxes. This is an improvement over inversions based on annual average data where the "rectification effect" causes erroneous compensating fluxes of order 0.7 GtC/year in Eurasia and North America. Table 3b shows that the differences in fossil CO_2 gradient between the two transport models cause erroneous terrestrial uptake in North America and Eurasia, because higher fossil CO_2 is simulated in the

Northern Hemisphere in GCTM than in SKYHI. A presumed terrestrial carbon sink in North America is well estimated by the inverse model (Table 3c). However, the differences between SKYHI and GCTM cause a presumed Eurasian sink of 1 GtC/year to be under estimated by 40 percent (Table 3d). These test inversions show what to expect about errors of the inverse calculations due to transport biases in a general sense, the results should not be extrapolated strictly (for instance, region by region) to inverse calculations with actual observations that resulted from real winds acting on real sources.

Table 3. Terrestrial NPP, RESP and net fluxes and oceanic uptake estimated by inverse modeling of monthly mean atmospheric CO_2 (data: NOAA CMDL network, flux unit: GtC/year, negative sign indicates flux out of the atmosphere).

(a) SKYHI model simulation of CASA net ecosystem production

Source Regions	CASA	NPP	RESP	Net	Expected
Global ocean				-0.3	0.0
Eurasia	8.9	-9.4	9.6	0.2	0.0
North America	6.2	-5.7	5.6	-0.1	0.0
Tropics & SH	33.8	-22.4	22.6	0.2	0.0

(b) SKYHI model simulation of CASA net ecosystem production + 1990 fossil fuel emissions + 1990 oceanic fluxes (Takahashi et al., 1997)

Source Regions	CASA	NPP	RESP	Net	Expected
Global ocean				-1.2	-1.1
Eurasia	8.9	-9.0	8.8	-0.2	0.0
North America	6.2	-5.6	4.9	-0.7	0.0
Tropics & SH	33.8	-22.9	24.0	1.1	0.0

(c) SKYHI model simulation of CASA net ecosystem production + a North American sink of 1 GtC/yr

Source Regions	CASA	NPP	RESP	Net	Expected
Global ocean				-0.3	0.0
Eurasia	8.9	-9.4	9.5	0.1	0.0
North America	6.2	-6.8	5.8	-1.0	-1.0
Tropics & SH	33.8	-25.6	25.7	0.1	0.0

(d) SKYHI model simulation of CASA net ecosystem production + a Eurasian sink of 1 GtC/yr

Source Regions	CASA	NPP	RESP	Net	Expected
Global ocean				-0.3	0.0
Eurasia	8.9	-10.3	9.7	-0.6	-1.0
North America	6.2	-5.8	5.7	-0.1	0.0
Tropics & SH	33.8	-21.3	21.3	0.0	0.0

The inversion results for monthly atmospheric CO_2 between 1993-1995 are shown in Table 4. The estimated annual NPP and RESP are each about 10-20 percent greater than predicted by the CASA model. Terrestrial carbon uptake was estimated for Eurasia and North America, each of size slightly over 1 GtC/year. Previously, we estimated, using an annual average inverse model, a large terrestrial uptake of carbon in North America, of about 1.5 GtC/year, between 1988-1992. A large terrestrial carbon source of 1.5-1.9 GtC/year is also estimated to be present in the region of Tropics and Southern Hemisphere. The present results are similar to that reported for the earlier period, and extend the mid-latitude Northern Hemispheric terrestrial carbon sink to a longer period of time.

Table 4. Terrestrial NPP, RESP and net fluxes estimated by inverse modeling of monthly mean atmospheric CO_2 (data: NOAA CMDL network, observations from 1993-1995, flux unit: GtC/year, negative sign indicates flux out of the atmosphere). The robust estimation method was used.

Source Regions	CASA	NPP	RESP	Net
Global ocean ^{a}				-2.2
Eurasia	8.9	-11.0	9.7	-1.3
North America	6.2	-8.3	7.2	-1.1
Tropics & SH	33.8	-0.8	2.7	1.9
Global ocean ^{b}				-2.1
Eurasia	8.9	-10.9	9.8	-1.1
North America	6.2	-8.7	7.4	-1.3
Tropics & SH	33.8	-7.5	9.0	1.5

^{a} Flux prescribed to Princeton ocean model.
^{b} Flux prescribed to Takahashi et al. (1999).

The terrestrial isotopic fluxes estimated by the inversion are shown in Table 5a for Eurasia and North America. The seasonal variations in the tropical region are so small that they do not provide sufficient information to allow a separate estimation of NPP and RESP (see Table 4). The isotopic fluxes divided by the estimated carbon fluxes give the isotopic fractionation coefficients during photosynthesis and the difference of isotopic ratios between atmospheric CO_2 and CO_2 released from soil organic matter (SOM). The estimated difference of isotopic ratios between the carbon reservoirs compares well with observations. If we assume a uniform isotopic fractionation coefficients of -20‰ for photosynthetic carbon assimilation, the isotopic fluxes can be

converted to carbon fluxes (NPP, RESP, and net, see Table 5b). The results for NPP and RESP are close to the estimates based on atmospheric CO_2 data. The atmospheric $\delta^{13}C$ data, which are independent of CO_2 measurements (although using the same air samples), appear to suggest for 1993-1995 a larger Eurasian carbon sink and a smaller North American carbon sink than implied by atmospheric CO_2 data. Year-by-year analysis indicates data from 1994 to be mostly responsible for the discrepancy (results not shown here). We will identify stations that "saw" the difference.

The isotopic fractionation coefficients vary significantly from boreal forest to temperate forest and to tropical savanna (Neil Suits, Colorado State University, personal communication). However, we did not have the terrestrial model results when the isotopic inverse model was constructed; we assumed uniform isotopic fractionations for the three large regions.

The modeled CO_2 mixing ratios and $\delta^{13}C$ values are compared to observations in Figure 5 for selected stations from north to south. At Barrow, Alaska, and Bermuda Island, the model lags the observation in the fall in CO_2 growth and in $\delta^{13}C$ decrease, while the seasonal amplitudes are in good agreement. By contrast, the model leads the observation by a month at Key Biscayne, Florida. Large residuals result from a mismatch of the seasonal phase between model and observation at many stations. At some stations in the North Pacific (Guam Island, Kumukahi, and Mauna Loa) the model underpredicts the seasonal amplitude, while at other stations (Midway, Shemya) the model agrees well with the observations. At stations located in the Southern Hemisphere (Samoa, South Pole), the model captures the long-term trend, but does not agree well in seasonal variability, although the seasonal fluctuations are small in the Southern Hemisphere. It appears that the dis-equilibrium isotopic fluxes in the Southern Ocean was over-estimated, causing a greater than observed decrease of atmospheric $\delta^{13}C$ at the South Pole, where the agreement is good for atmospheric CO_2 mixing ratio. As land biomes are small in size in the extra-tropical Southern Hemisphere, seasonal changes in ocean biology and sea surface temperature can cause

atmospheric CO_2 and $\delta^{13}C$ variations comparable in size to that due to terrestrial ecosystems.

Table 5a. Terrestrial NPP and RESP fluxes estimated by inverse modeling of monthly mean atmospheric CO_2 and $\delta^{13}C$ of CO_2 (data: NOAA CMDL network, observations from 1993-1995, negative sign indicates flux out of the atmosphere)

Source Regions	Flux	GtC/yr	‰GtC/yr	ε (‰)
Eurasia	NPP	-11.0	220.0	-20.0
	RESP	9.7	-188.0	-19.4
North America	NPP	-8.3	161.7	-19.5
	RESP	7.2	-148.0	-20.6

Note: Oceanic fluxes of CO_2 and $^{13}CO_2$ were prescribed according to the Princeton ocean biogeochemistry model.

Table 5b. Terrestrial NPP and RESP fluxes estimated by inverse modeling of monthly mean atmospheric CO_2 and $\delta^{13}C$ of CO_2 (data: NOAA CMDL network, observations from 1993-1995, negative sign indicates flux out of the atmosphere)

Source Regions	Flux	‰GtC/yr	GtC/yr #
Eurasia	NPP	220.0	-11.0
	RESP	-188.0	9.4
	Net	32.0	-1.6
North America	NPP	161.7	-8.1
	RESP	-148.0	7.4
	Net	13.7	-0.7

Note: Oceanic fluxes of CO_2 and $^{13}CO_2$ were prescribed according to the Princeton ocean biogeochemistry model. #Assume ε = -20‰ and assume there is no disequilibrium between soil respired CO_2 and the atmosphere.

Our prescribed ocean fluxes are based on annual average ocean model results, and therefore do not have seasonal variations. Furthermore, we did not consider interannual variabilities in our inverse model. The model and data comparison can be improved by fitting to data one year at a time, and using ocean fluxes with a seasonal resolution.

4. Future Work

There are two areas for improvement in the inverse model. First, we need accurate and seasonally resolved oceanic fluxes of carbon isotopes. Synthesis of ocean measurements obtained during JGOFS and WOCE programs will provide new observational constraints on the air-sea exchange. New ocean biogeochemistry models are under development that use improved ocean circulation and ocean biology. Secondly, we need realistic representation of the spatial and temporal variations of terrestrial carbon isotopes fluxes. A new terrestrial biogeochemistry model of carbon cycle is under development at Colorado State University, and will provide improved terrestrial "basis functions" for our inverse model.

Acknowledgments: We thank Bob Andres (University of Alaska Fairbanks) for producing the monthly isotopic ratios maps for the US fossil fuel carbon emissions and annual maps for the world. The observations of atmospheric CO_2 and $\delta^{13}C$ ratio of CO_2 were made by the NOAA CMDL (directed by Pieter Tans) in colaboration with the INSTARR University of Colorado (directed by Jim White). Computational resource and the atmospheric transport models were provided to us by GFDL, courtesy of Jerry Mahlman.

References

Andres, R.J., G. Marland, I. Fung, and E. Matthews, A 1° x 1° distribution of carbon dioxide emissions from fossil fuel consumption and cement manufacture, 1950-1990, *Global Biogeochemical Cycles, 10*, 419-429, 1995.

Fan, S., M. Gloor, J. Mahlman, S. Pacala, J. Sarmiento, T. Takahashi, and P. Tans, A large terrestrial carbon sink in North America implied by atmospheric and oceanic CO_2 data and models, *Science, 282*, 442-446, 1998.

Gloor, M., S.-M. Fan, S.W. Pacala, J. L. Sarmiento, and M. Ramonet, A model-based evaluation of inversions based on atmospheric transport, using annual mean mixing ratios, as a tool to monitor fluxes of nonreactive trace substances like CO2 on a continental scale, *Journal of Geophysical Research, 104*, 14,245-14,260, 1999.

Gloor, M., S.-M. Fan, S.W. Pacala, and J. L. Sarmiento, Optimal sampling of the atmosphere for purpose of inverse modeling - a model study, *Global biogeochemical Cycles, 14*, 407-428, 2000.

Murnane, R.J., and J.L. Sarmiento, Roles of biology and gas exchange in determining the $\delta^{13}C$ distribution in the ocean and the preindustrial gradient in atmospheric $\delta^{13}C$, *Global biogeochemical Cycles, 14*, 389-405, 2000.

Murnane, R.J., J.L. Sarmiento, and C. Le Quere, Spatial distribution of air-sea CO_2 fluxes and the interhemispheric transport of carbon by the oceans, *Global Biogeochemical Cycles, 13*, 287-305, 1999

Potter, C.S., et al., Terrestrial ecosystem production: A process model based on global satellite and surface data, *Global biogeochemical Cycles, 7*, 811-841, 1993.

Press, W.H., S.A. Teukolsky, W.T. Vetterling, and B.P. Flannery, *Numerical Recipes in C, The Art of Scientific Computing*, second edition, Cambridge University Press, 1992.

Takahashi, T., R.A. Feely, R. Weiss, R.H. Wanninkhof, D.W. Chipman, S.C. Sutherland, and T. Takahashi, Global air-sea flux of CO_2: An estimate based on measurements of sea-air pCO_2 difference, *Proceedings of the National Academy of Sciences, U.S.A., 94*, 8292-8299, 1997.

Tans, P.P. I.Y. Fung, and T. Takahashi, Observational constraints on the global atmospheric CO2 budget, *Science, 247*, 1431-1438, 1990.

Figure Captions

Figure 1. A world map of carbon isotopic ratios of fossil CO_2 released by each nation.

Figure 2. A U.S. map of isotopic ratios of fossil CO_2 released by each state in 1995. (a) January, (b) July.

Figure 3. A map of terrestrial source regions defined for the inverse model.

Figure 4. Zonal average $\delta^{13}C$ caused by fossil emissions and oceanic fluxes, shown as deviations from January value at the Sout Pole Observatory.

Figure 5. Comparison of observations and post-inversion model predictions at selected stations.

Fig. 1

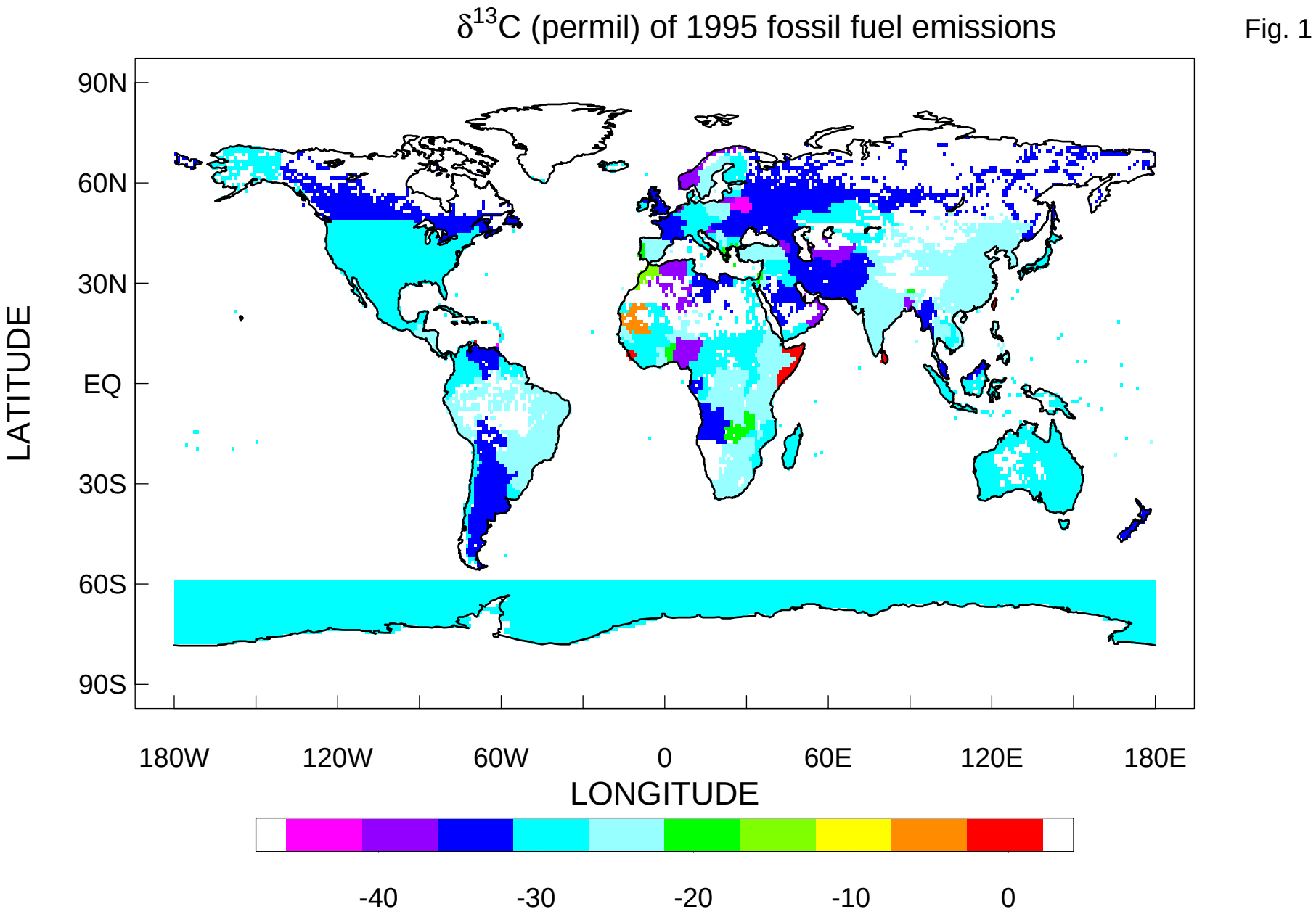
δ13C (permil) of 1995 fossil fuel emissions
90N
60N
30N
EQ
30S
60S
90S
LATITUDE
180W
120W
60W
0
60E
120E
180E
LONGITUDE
-40
-30
-20
-10
0

Fig. 2a

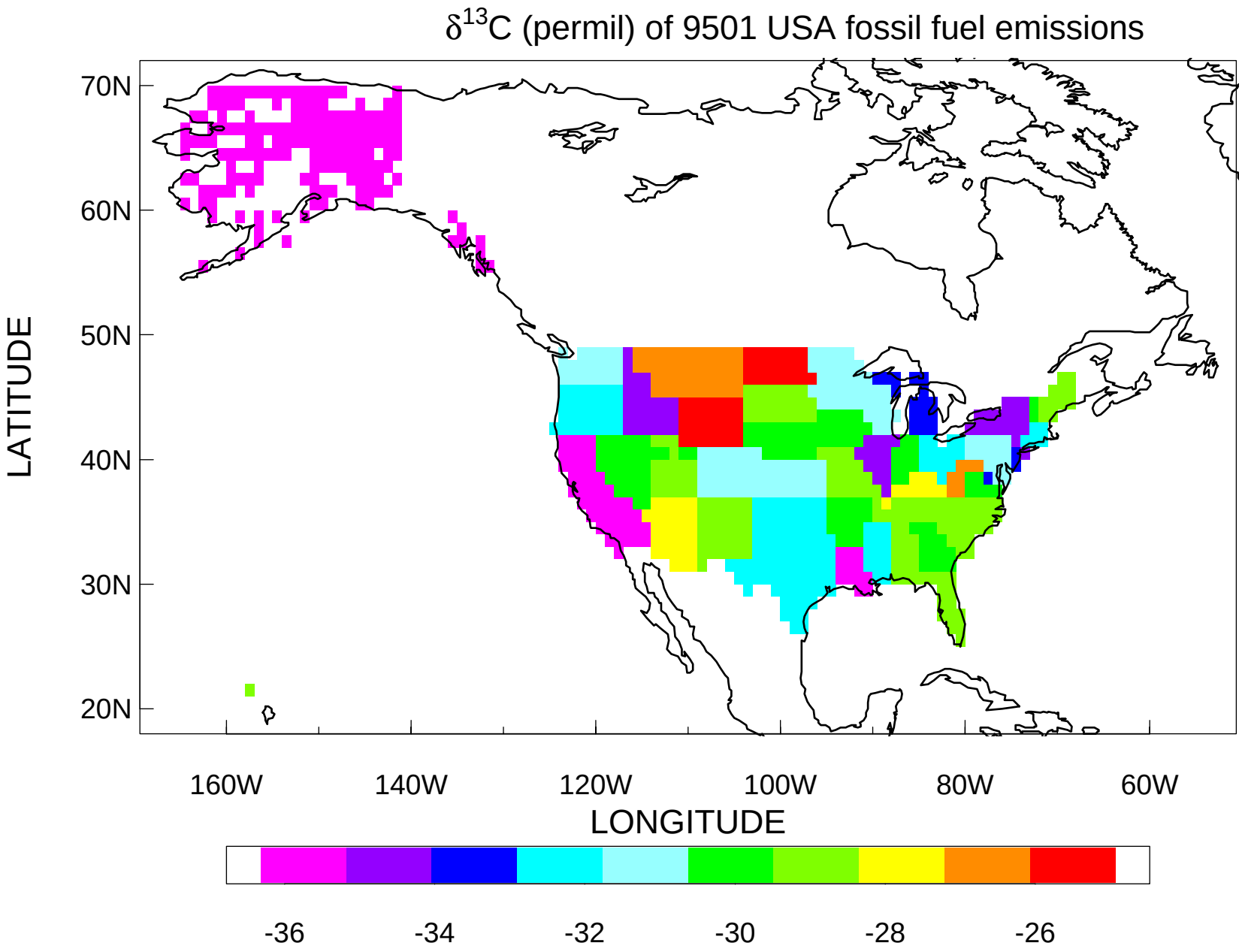
δ13C (permil) of 9501 USA fossil fuel emissions
70N
60N
50N
40N
30N
20N
LATITUDE
160W
140W
120W
100W
80W
60W
LONGITUDE
-36
-34
-32
-30
-28
-26

Fig. 2b

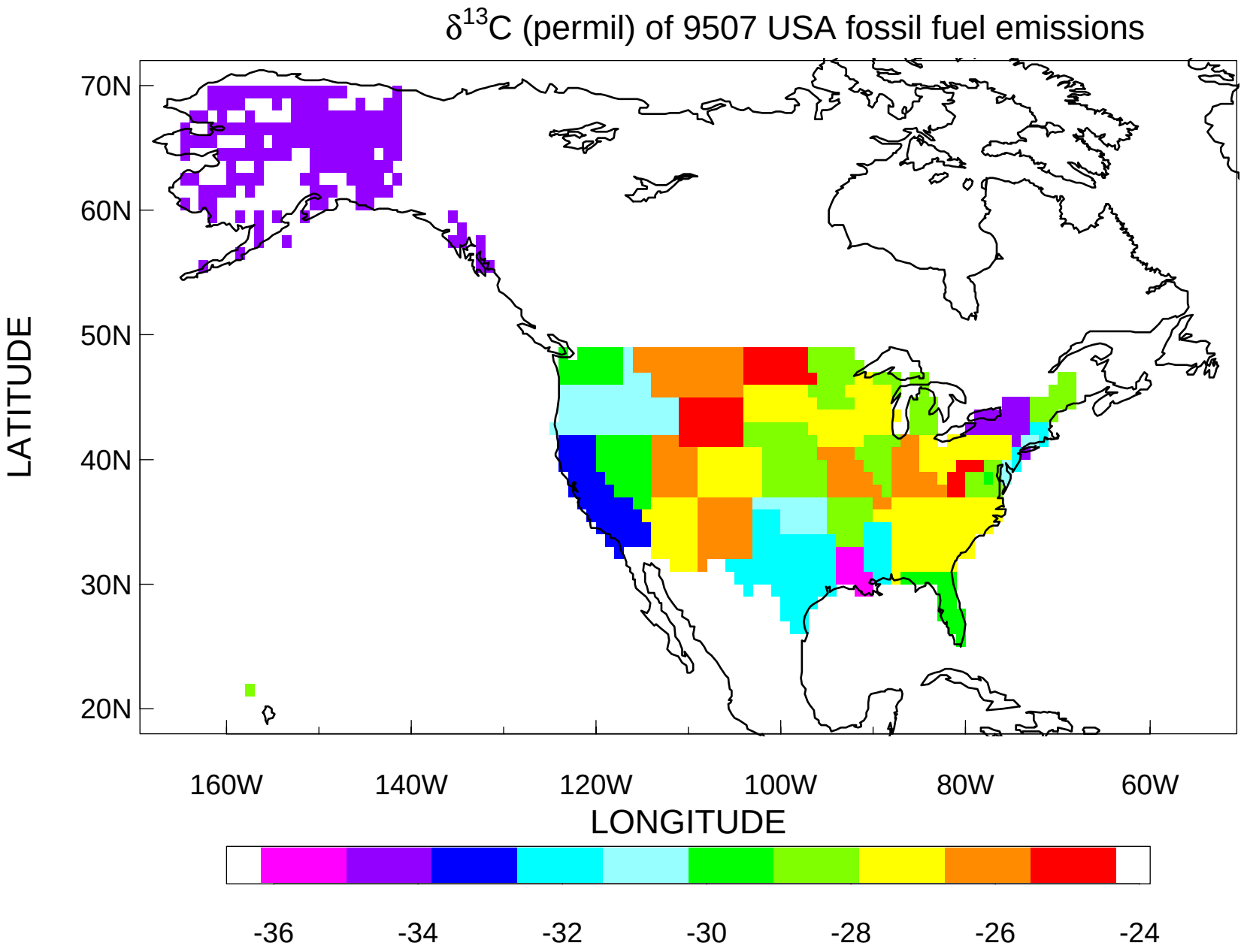
δ13C (permil) of 9507 USA fossil fuel emissions
70N
60N
50N
40N
30N
20N
LATITUDE
160W
140W
120W
100W
80W
60W
LONGITUDE
-36
-34
-32
-30
-28
-26
-24

Fig. 3

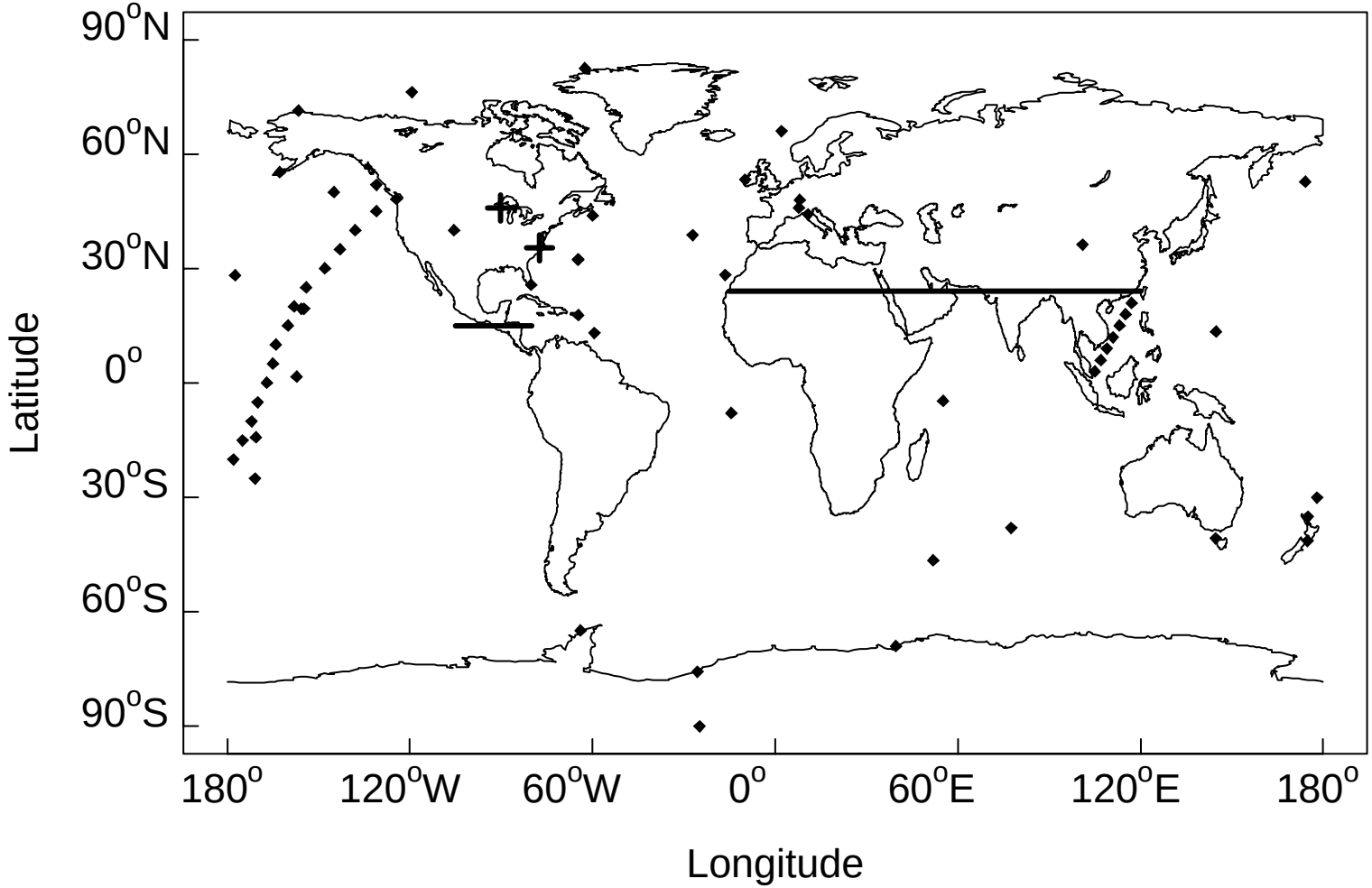
90°N
60°N
30°N
0°
30°S
60°S
90°S
Latitude
180°
120°W
60°W
0°
60°E
120°E
180°
Longitude

Annual Zonal Mean in Atmopsheric Surface Layer

Fig. 4

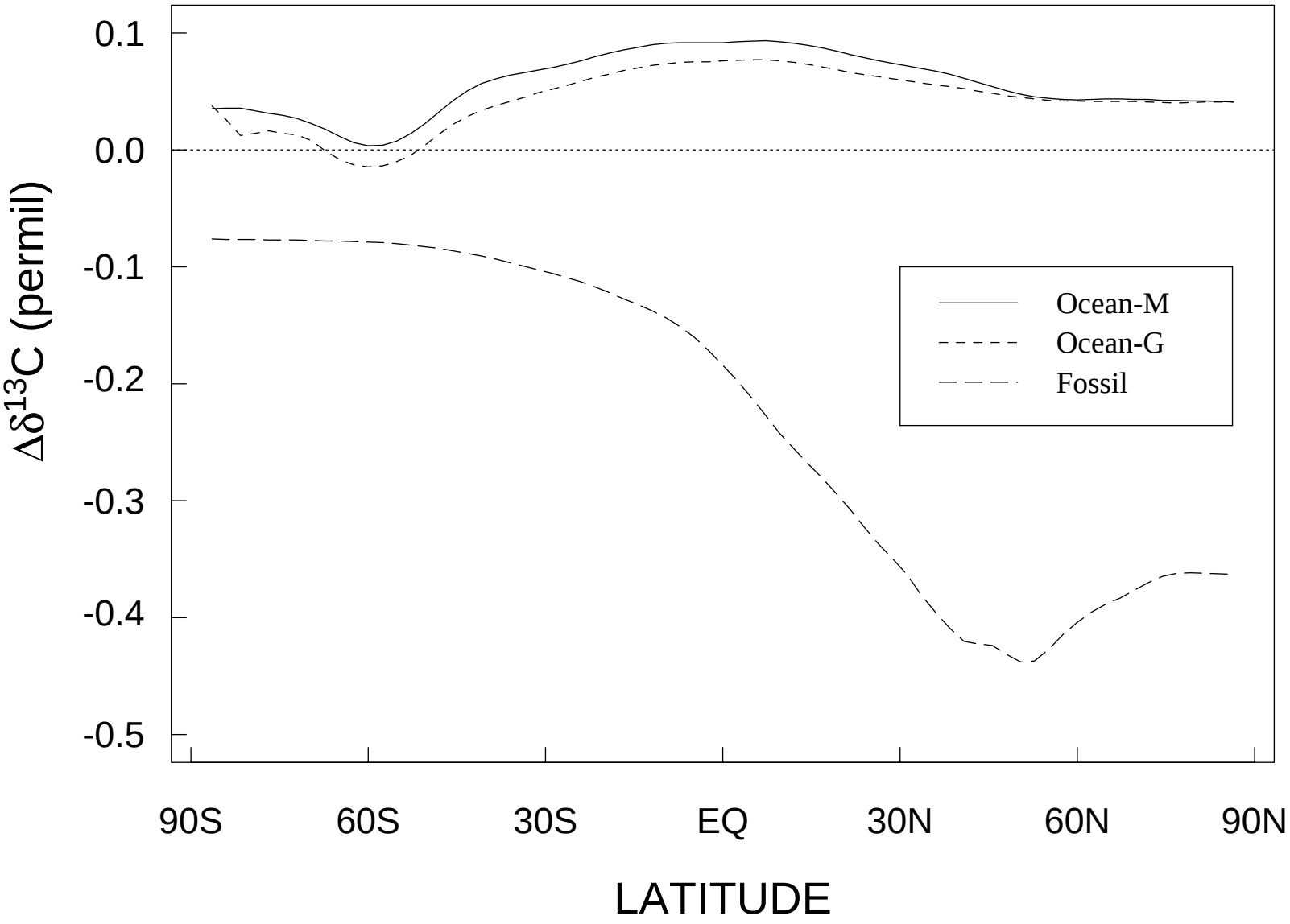

Fig. 5a

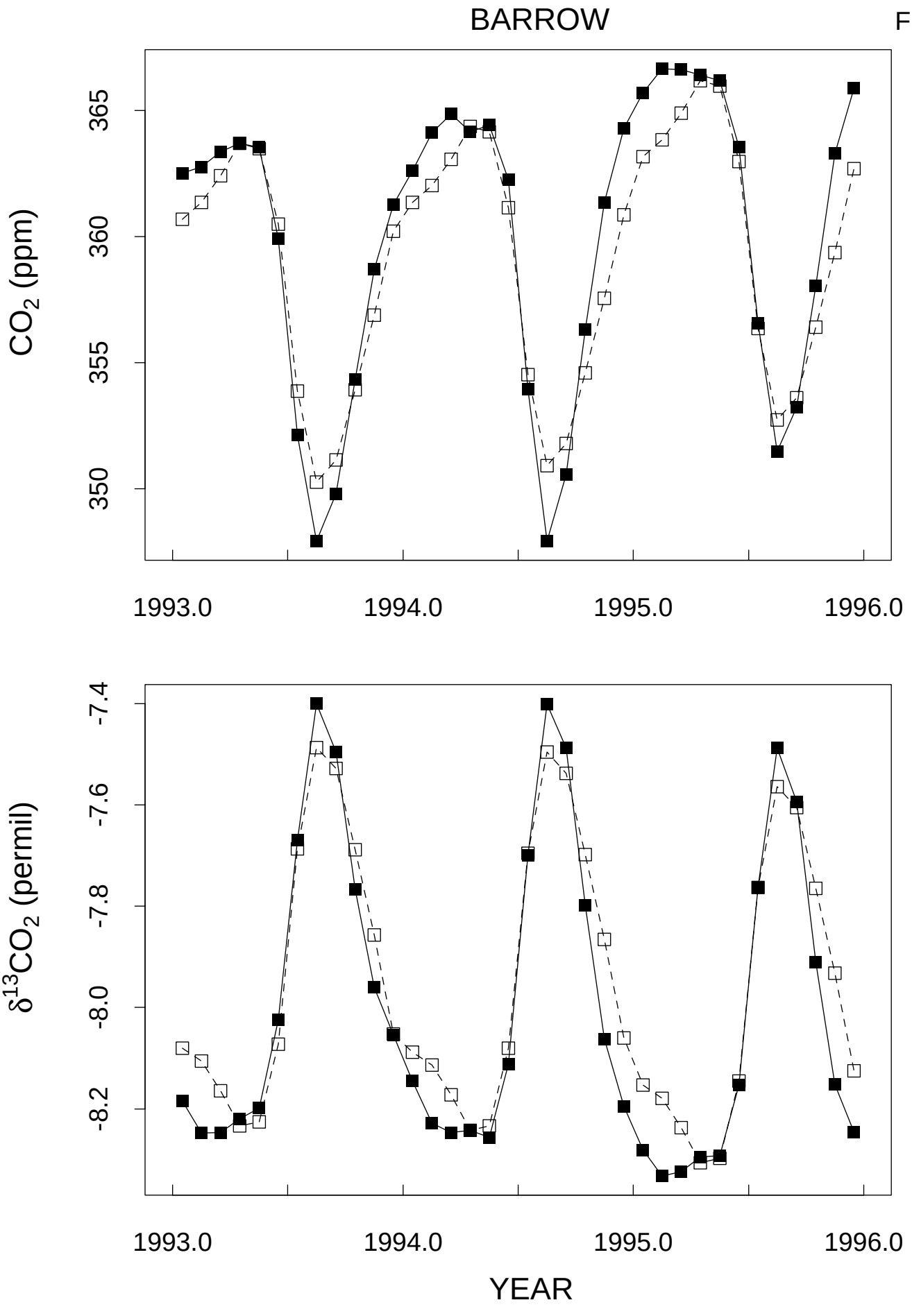
BARROW
CO2 (ppm)
365
360
355
350
1993.0
1994.0
1995.0
1996.0
δ13CO2 (permil)
-7.4
-7.6
-7.8
-8.0
-8.2
1993.0
1994.0
1995.0
1996.0
YEAR

Fig. 5b

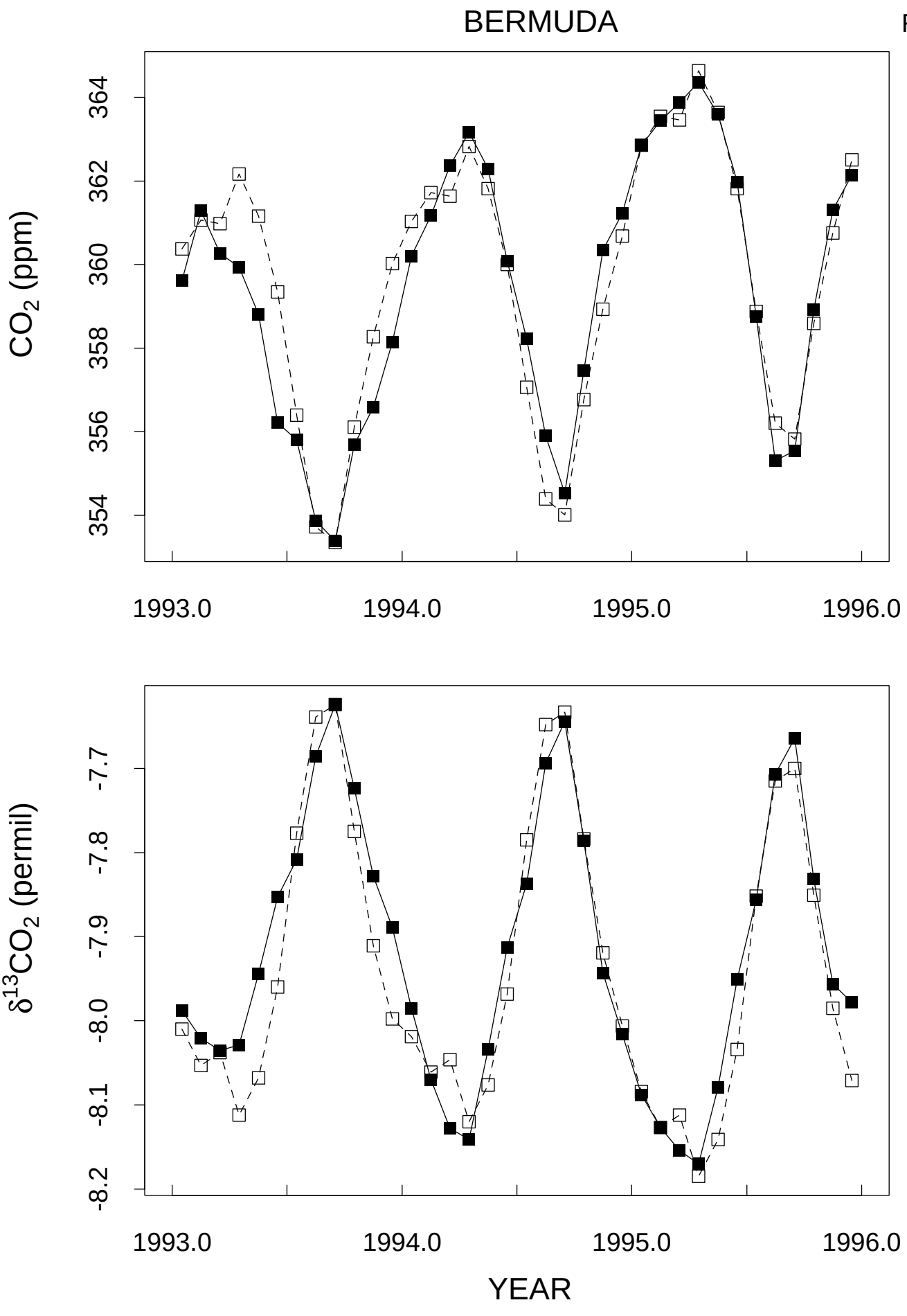
BERMUDA
CO_2 (ppm)
364
362
360
358
356
354
1993.0
1994.0
1995.0
1996.0
$\delta^{13}CO_2$ (permil)
-7.7
-7.8
-7.9
-8.0
-8.1
-8.2
1993.0
1994.0
1995.0
1996.0
YEAR

KEY BISCAYNE

Fig. 5c

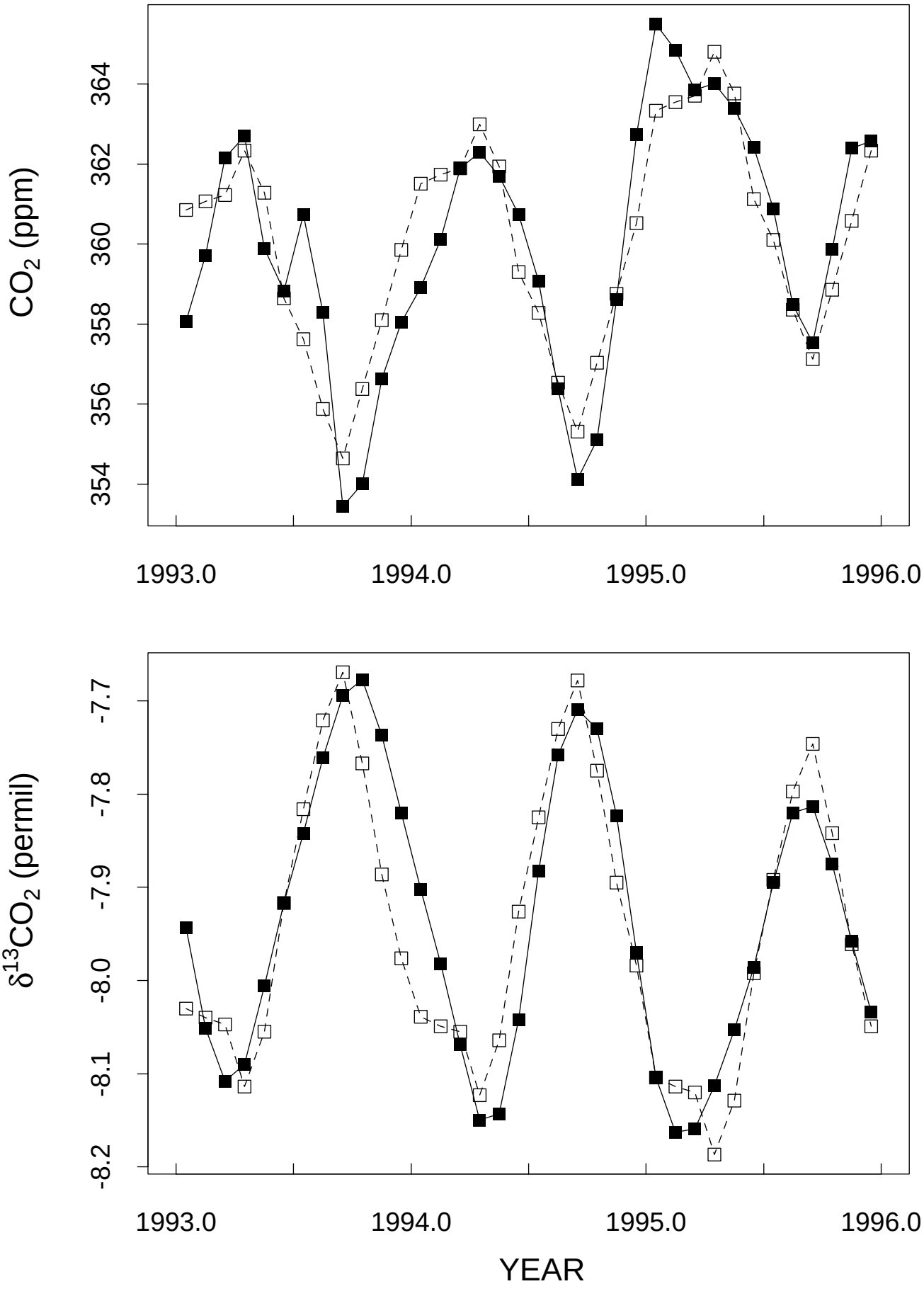

GUAM ISLAND

Fig. 5d

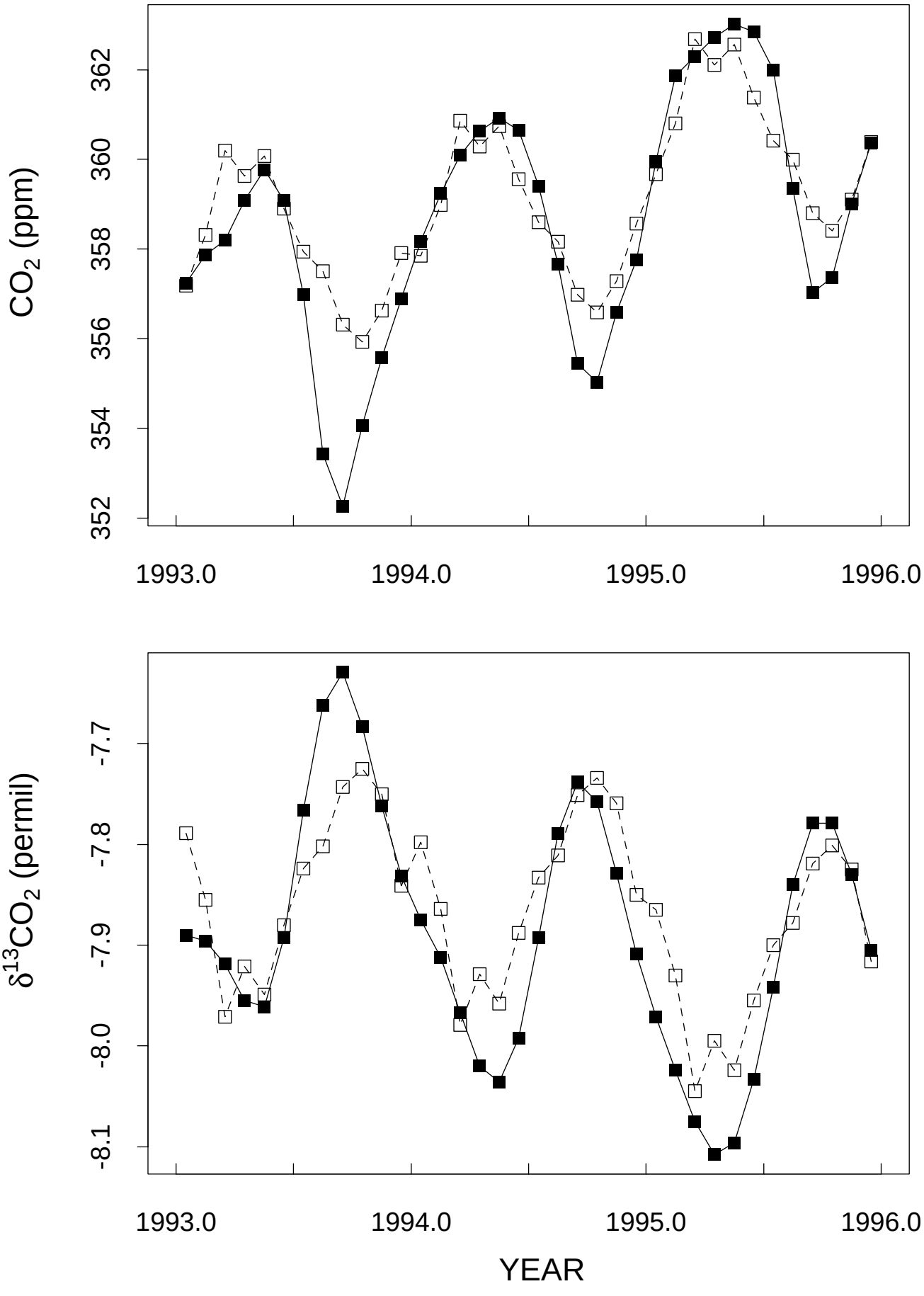

KUMUKAHI

Fig. 5e

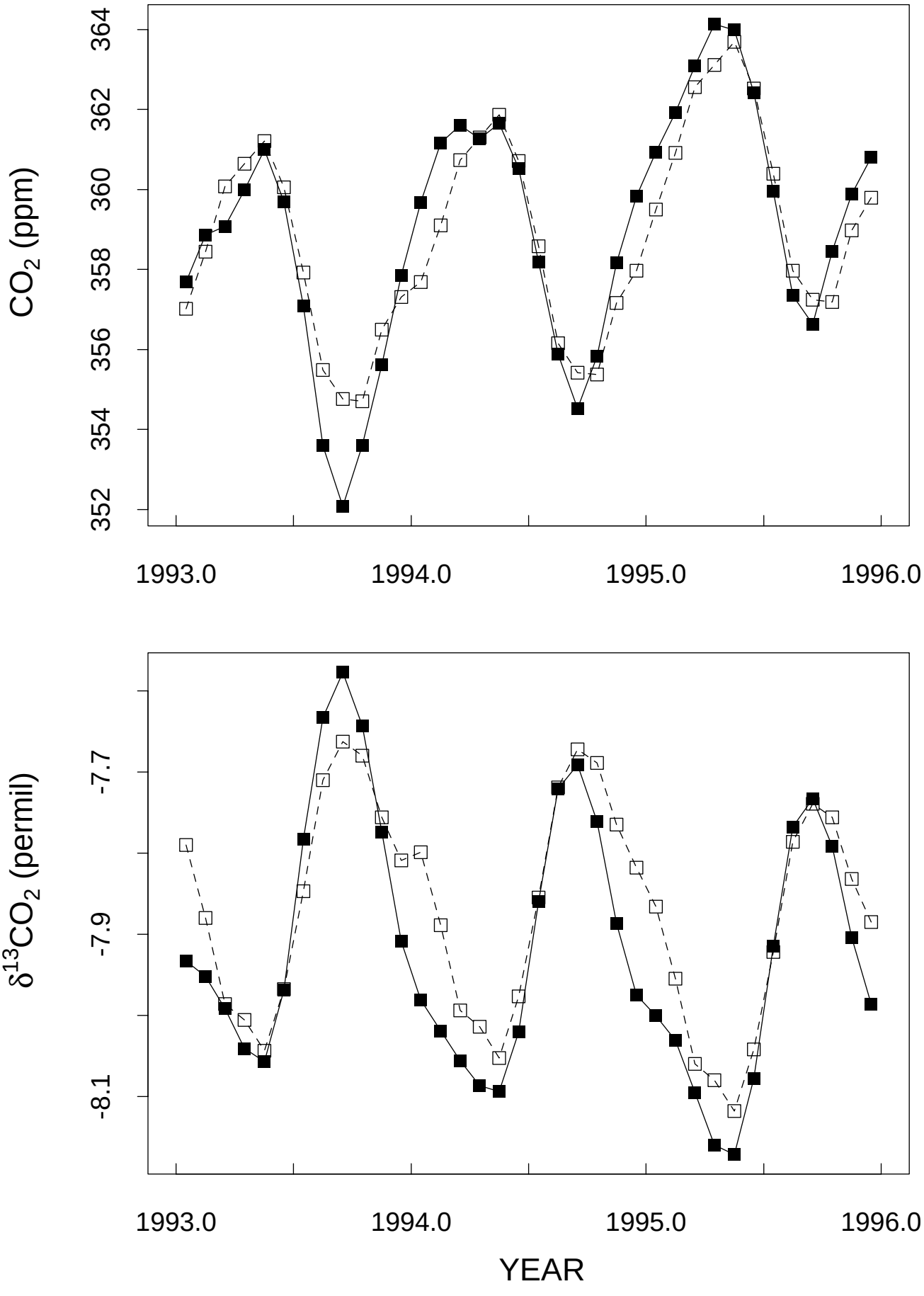

Fig. 5f

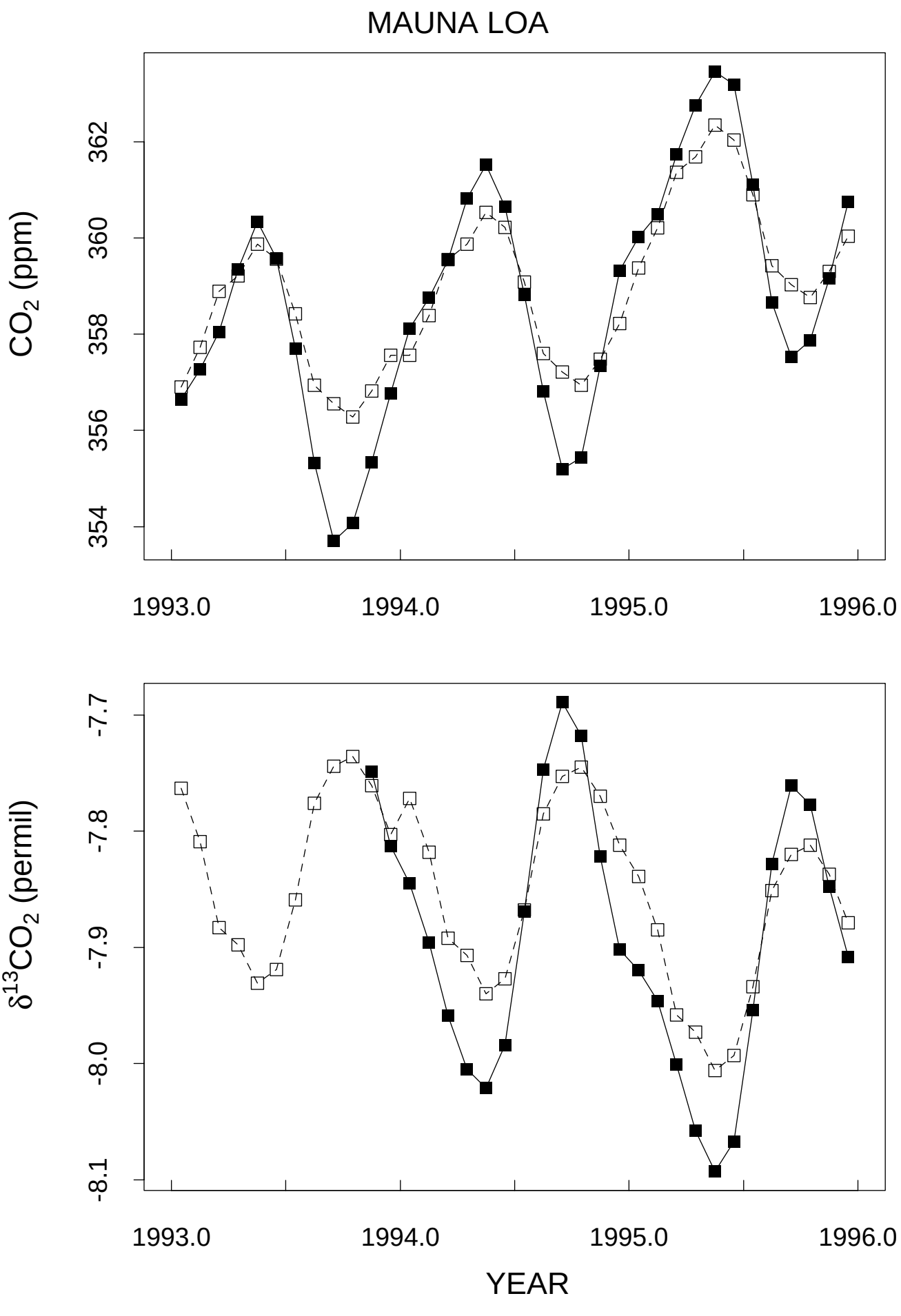
MAUNA LOA
CO2 (ppm)
354
356
358
360
362
δ13CO2 (permil)
-8.1
-8.0
-7.9
-7.8
-7.7
1993.0
1994.0
1995.0
1996.0
YEAR

Fig. 5g

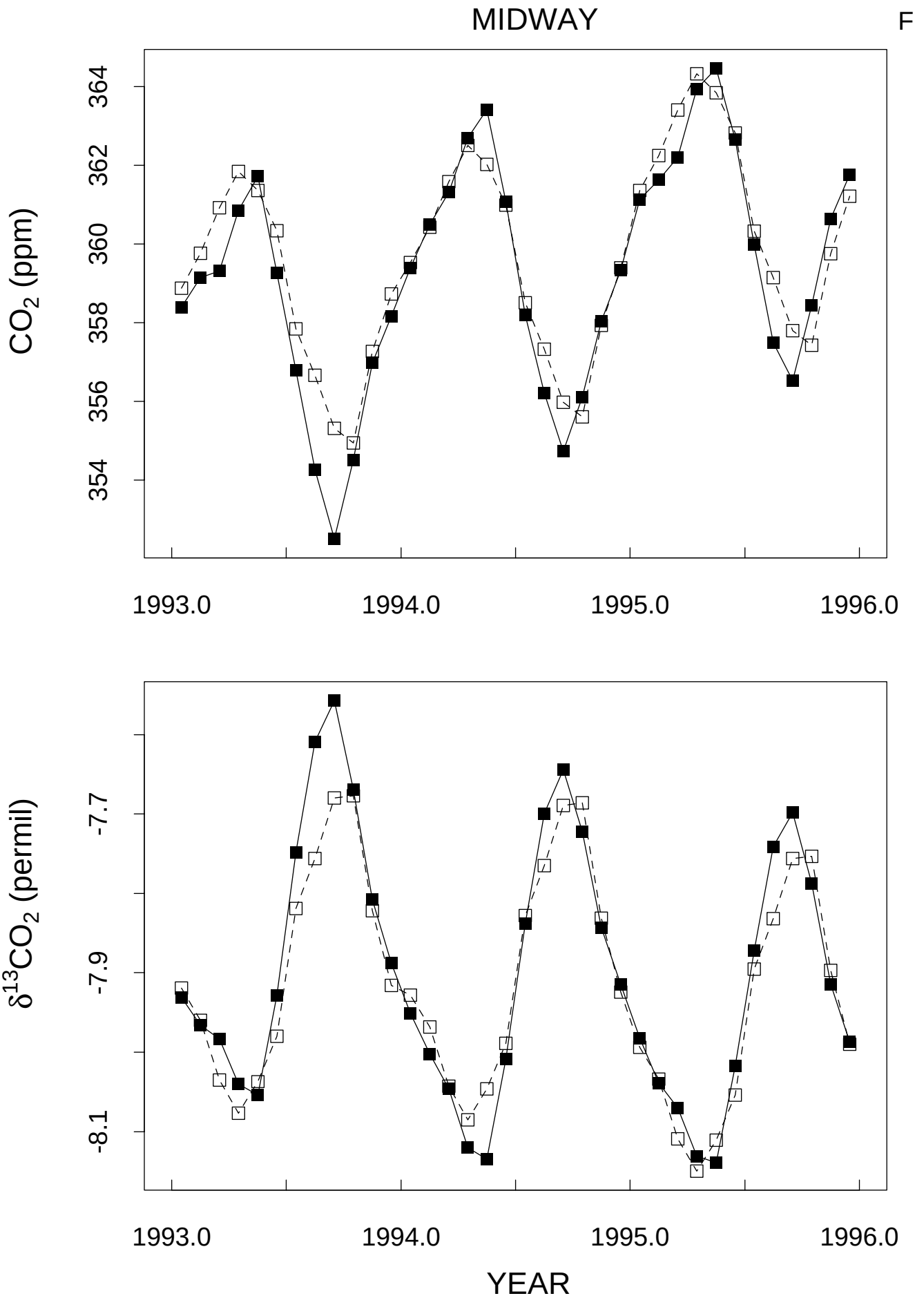
MIDWAY
CO_2 (ppm)
364
362
360
358
356
354
1993.0
1994.0
1995.0
1996.0
$\delta^{13}CO_2$ (permil)
-7.7
-7.9
-8.1
1993.0
1994.0
1995.0
1996.0
YEAR

SHEMYA

Fig. 5h

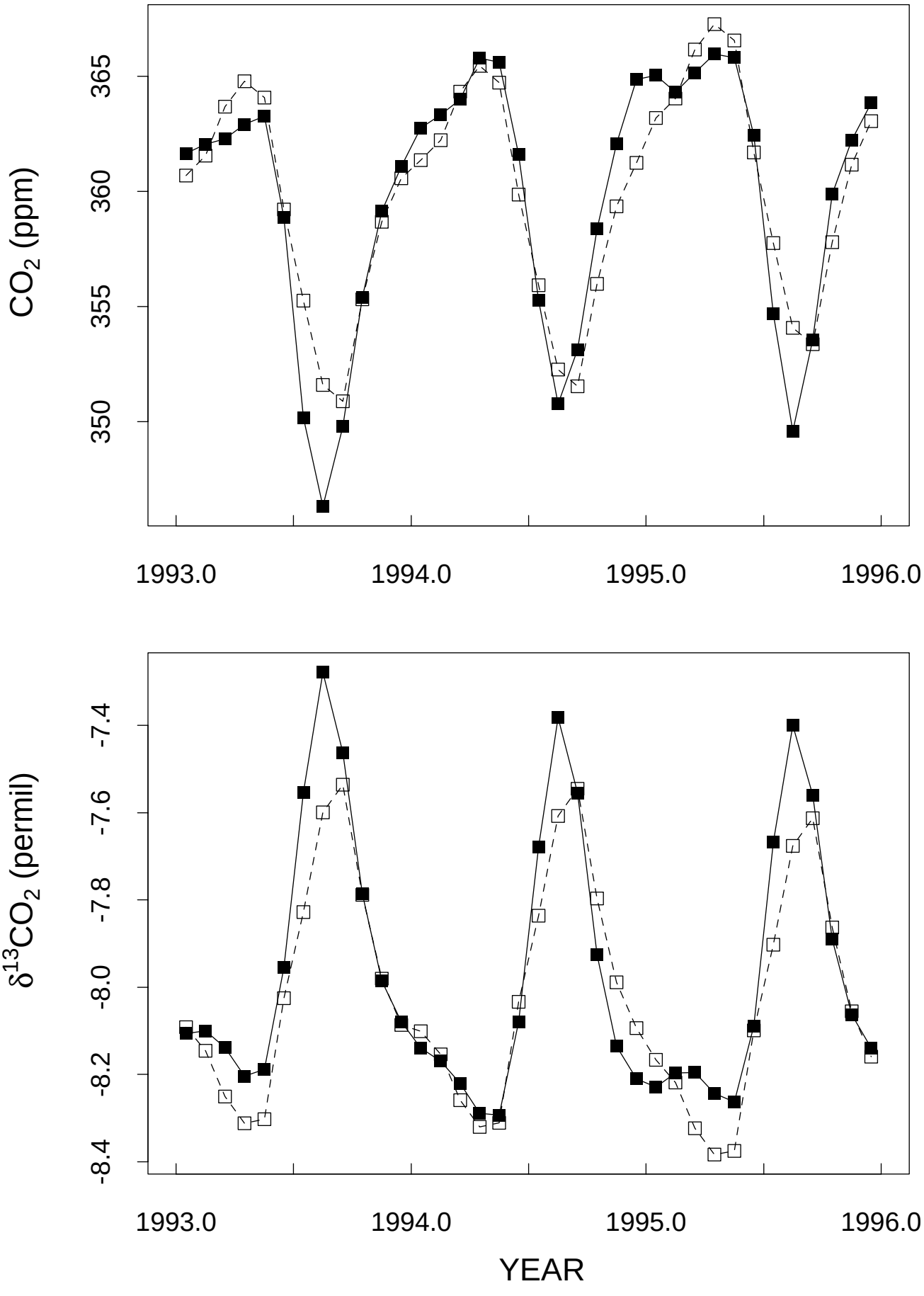

Fig. 5i

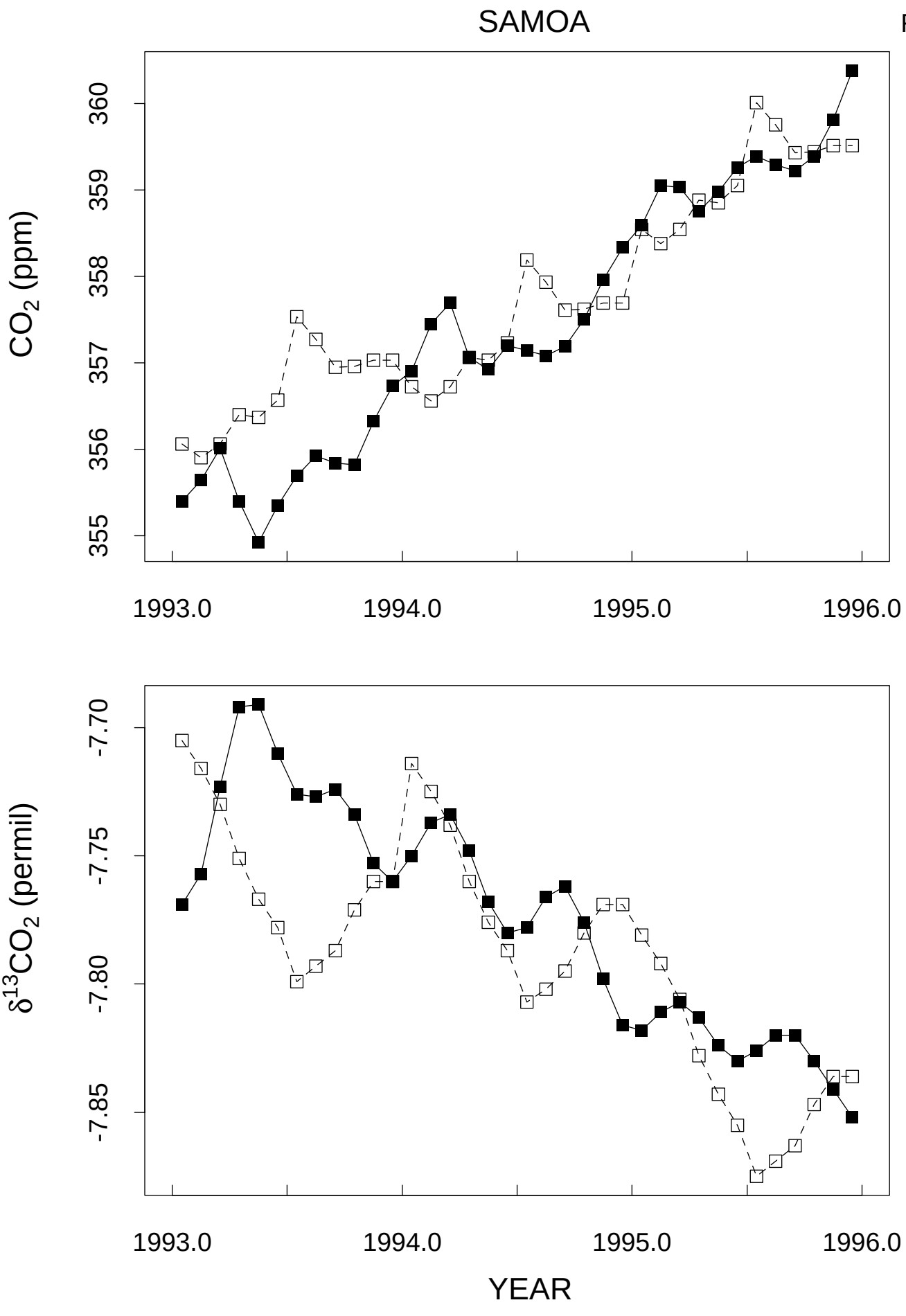
SAMOA
CO_2 (ppm)
355
356
357
358
359
360
1993.0
1994.0
1995.0
1996.0
$\delta^{13}CO_2$ (permil)
-7.85
-7.80
-7.75
-7.70
1993.0
1994.0
1995.0
1996.0
YEAR

Fig. 5j

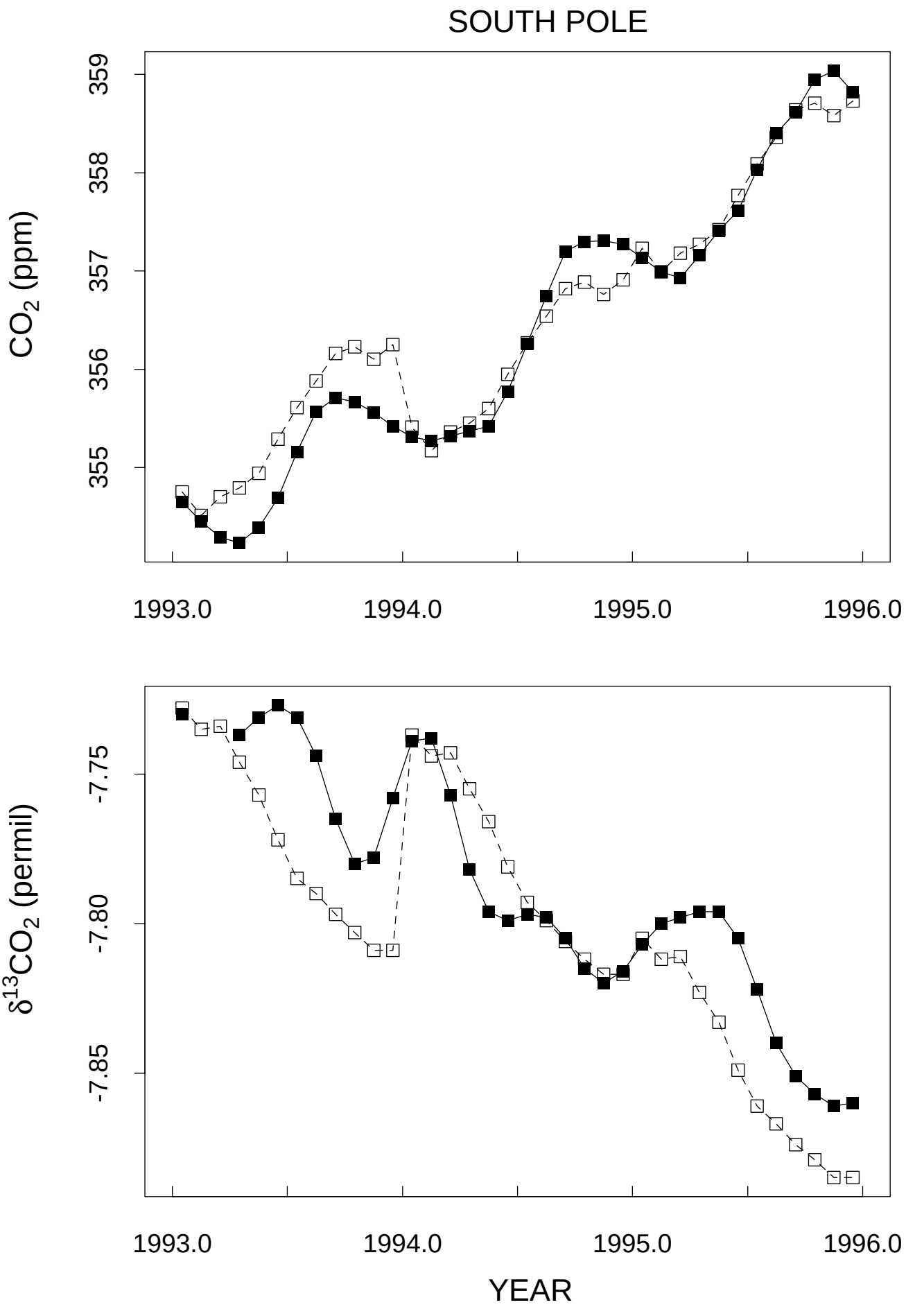
SOUTH POLE
CO2 (ppm)
359
358
357
356
355
1993.0
1994.0
1995.0
1996.0
δ13CO2 (permil)
-7.75
-7.80
-7.85
1993.0
1994.0
1995.0
1996.0
YEAR